frontiers | Frontiers in Water

ORIGINAL RESEARCH
published: 25 April 2022
doi: 10.3389/frwa.2022.874240

Mass- and Energy-Balance Modeling and Sublimation Losses on Dokriani Bamak and Chhota Shigri Glaciers in Himalaya Since 1979

*Smriti Srivastava and Mohd. Farooq Azam**

Department of Civil Engineering, Indian Institute of Technology Indore, Indore, India

Available surface energy balance (SEB) studies on the Himalayan glaciers generally investigate the melt-governing energy fluxes at a point-scale. Further, the annual glacier-wide mass balance (B_a) reconstructions have often been performed using temperature-index (T-index) models. In the present study, a mass- and energy-balance model is used to simulate the B_a on Dokriani Bamak Glacier (DBG, central Himalaya) and Chhota Shigri Glacier (CSG, western Himalaya) using the bias-corrected ERA5 data from 1979 to 2020. The model is calibrated using *in-situ* B_a and validated against available *in-situ* altitudinal and geodetic mass balances. DBG and CSG show mean B_a of -0.27 ± 0.32 and -0.31 ± 0.38 m w.e. a^{-1} (meter water equivalent per year), respectively, from 1979 to 2020. Glacier-wide net shortwave radiation dominates the SEB followed by longwave net radiation, latent heat flux, and sensible heat flux. The losses through sublimation are around 22% on DBG and 20% on CSG to the total ablation with a strong spatial and temporal variability. Modeled B_a is highly sensitive to snow albedo —with sensitivities of 0.29 and 0.37 m w.e. a^{-1} for 10% change in the calibrated value—on DBG and CSG, respectively. The sensitivity of the modeled mean B_a to 1°C change in air temperature and 10% change in precipitation, respectively is higher on DBG (-0.50 m w.e. $a^{-1}{}^{\circ}C^{-1}$, 0.23 m w.e. a^{-1}) than the CSG (-0.30 m w.e. $a^{-1}{}^{\circ}C^{-1}$, 0.13 m w.e. a^{-1}). This study provides insights into the regional variations in mass-wastage governing SEB fluxes at a glacier-wide scale, which is helpful for understanding the glacier–climate interactions in the Himalaya and stresses an inclusion of sublimation scheme in T-index models.

Keywords: Himalaya, glacier wastage, glacier surface energy balance, glacier-climate interactions, mass balance sensitivity

OPEN ACCESS

Edited by:
Riyaz Ahmad Mir,
Geological Survey of India, India

Reviewed by:
Manish Pandey,
Chandigarh University, India
Rijan Bhakta Kayastha,
Kathmandu University, Nepal
Sher Muhammad,
International Centre for Integrated Mountain Development, Nepal

****Correspondence:***
Mohd. Farooq Azam
farooqazam@iiti.ac.in;
farooqaman@yahoo.co.in

Specialty section:
This article was submitted to Water and Climate, a section of the journal Frontiers in Water

Received: *11 February 2022*
Accepted: *17 March 2022*
Published: *25 April 2022*

Citation:
Srivastava S and Azam MF (2022) Mass- and Energy-Balance Modeling and Sublimation Losses on Dokriani Bamak and Chhota Shigri Glaciers in Himalaya Since 1979. Front. Water 4:874240. doi: 10.3389/frwa.2022.874240

INTRODUCTION

Himalaya-Karakoram (HK), also known as the Third Pole, is among the most vulnerable water towers on Earth (Immerzeel et al., 2020). Glaciers in the HK region generate the headwaters of the South Asian River Systems including the Indus, the Ganga, and the Brahmaputra (Bolch et al., 2019). These River Systems quench the water requirements for irrigation, hydropower, and the industrial needs of more than a billion people who live in the neighboring countries of India (Azam et al., 2021). Due to increasing temperatures and erratic precipitation patterns (Bolch et al., 2019; Hock et al., 2019; Krishnan et al., 2019), the HK glaciers are at risk. Studies suggest a spatially heterogeneous glacier wastage in the High Mountains of Asia (Kääb et al., 2015; Brun et al., 2017; Shean et al., 2020) including the HK region (Azam et al., 2018). In response to regional and global

warming (Banerjee and Azam, 2016; Kraaijenbrink et al., 2017), the Himalayan glaciers have been losing their mass over the last 6 to7 decades, similar to the other glaciers, worldwide (Azam et al., 2018). However, the Karakoram glaciers have been in a near-balanced state due to a phenomenon termed, "Karakoram Anomaly" since the 1970s (Bolch et al., 2017; Berthier and Brun, 2019), (Hewitt, 2005; Gardelle et al., 2012). Some recent studies indicate a slight mass loss in the ablation zones (Muhammad and Tian, 2016) and throughout the Karakoram region in the early twenty-first century (Muhammad et al., 2019). Emerging evidence infers that the exceptional behavior of the Karakoram Glaciers might be linked with increasing local irrigation (de Kok et al., 2018) that results in increased snowfalls over the Karakoram range, thereby balancing mass budgets (Kumar et al., 2019). Recent findings also suggest that Karakoram Anomaly is centered on the western Kunlun and eastern Pamir (Kääb et al., 2015; Brun et al., 2017). Nevertheless, our understanding of the Karakoram Anomaly is under progress and needs further investigation (Farinotti et al., 2020).

Long-term annual glacier wide mass balance (B_a) measurements are necessary to comprehend the climate change effects, especially in the inaccessible regions, such as HK where high-altitude meteorological measurements are sparse and our interpretation of the climate–glacier relationship is still limited (Shea et al., 2015a; Azam et al., 2018; Bolch et al., 2019). The classical glaciological method (Østrem and Brugman, 1991) is used to observe glacier mass changes at annual or seasonal scales that can directly be interpreted as undelayed feedback due to meteorological changes (Oerlemans, 2001). Measurements of B_a in the HK region are logistically challenging due to rugged topography, extreme climate, and high expedition cost; consequently, measurements have been conducted only on 26 glaciers, covering approximately 112 km^2 (out of total 39,000 glaciers in the HK) (Azam et al., 2018). Further, B_a measurements using the glaciological method are available for very short periods, generally <10 years, and cannot be used to understand how glaciers respond to climate change (Azam et al., 2018).

Accelerated progress in satellite data collection and processing, and open access to recently released stereo pairs from spy satellites and precise laser altimetry (ICESat) data have offered many geodetic mass change estimates at the glacier- and regional-wide scale over the last two decades (Muhammad and Tian, 2016, 2020; Brun et al., 2017; Vijay and Braun, 2018; Berthier and Brun, 2019; Maurer et al., 2019; Rashid and Majeed, 2020; Shean et al., 2020). An advantage of remote sensing tools is their large areal coverage, but the geodetic estimates cannot be interpreted directly to comprehend changes in climate as they are available at a multiannual scale and provide an average response of glaciers over several years.

In this situation, an alternative tool is to use glacier mass balance models to compute the long-term annual or seasonal B_a, and understand their climate change responses (Oerlemans et al., 1998; Vincent et al., 2004; Huss et al., 2008; Pellicciotti et al., 2008; Azam et al., 2014a). For long-term mass balance reconstructions, models exploit the available short-term *in-situ* mass balance and meteorological data together with long-term gridded meteorological and satellite data (Fujita et al., 2011; Zhang et al., 2011; Azam et al., 2014a; Sunako et al., 2019). Several studies have been performed to reconstruct the mass balances in the HK region at a glacier-wide scale (Brun et al., 2015; Kumar et al., 2016, 2020; Azam et al., 2019; Azam and Srivastava, 2020) and a region-wide scale (Shea et al., 2015b; Tawde et al., 2017; Kumar et al., 2019).

Brun et al. (2015) measured the seasonal changes of glacier surface albedo on CSG (Himachal Pradesh, India) and Mera (Khumbu Region, Nepal) glaciers using remote sensing data and reconstructed the B_a over 1999–2013 using a surface albedo model. A few studies developed a simplified temperature-index (T-index) model and reconstructed the long-term B_a on CSG and Shaune Garang (western Himalaya), DBG (central Himalaya), and Siachen (Karakoram) glaciers (Kumar et al., 2016, 2020; Engelhardt et al., 2017; Azam et al., 2019; Azam and Srivastava, 2020) over the last 4 to 5 decades. Tawde et al. (2017) developed a model by combining the T-index model, accumulation-area ratio (AAR) method, and satellite-derived snowlines, and estimated a mean mass wastage of -0.61 ± 0.46 m w.e. a^{-1} for 146 glaciers over 1984–2012 in the Chandra Basin (western Himalaya). Shea et al. (2015b) used a more sophisticated T-index model including snow redistribution, avalanche contribution, and glacier dynamics, and estimated a volume loss of -6.4 ± 1.5 km^3 for the Dudh Koshi Basin over 1961–2007.

Due to limited *in-situ* glacio-meteorological data, the available studies often used the simplified T-index, AAR, and surface albedo approaches for the B_a reconstructions in the HK region. Such simplified approaches often perform well but cannot estimate the sublimation losses, suggested to be significant in the HK region (Azam et al., 2021). The application of surface energy balance (SEB)-based mass balance models—explaining the physical basis of glacier mass balance—have been applied on a few glaciers (Kayastha et al., 1999; Fujita and Sakai, 2014; Patel et al., 2021).

In the present study, we applied a mass- and energy-balance model to simulate the B_a on two climatically contrasting glaciers of DBG (central Himalaya) and CSG (western Himalaya), where relatively good field observations are available (Azam et al., 2018). The selected glaciers are reference glaciers in the HK (Azam, 2021). The model is forced with long-term, bias-corrected meteorological ERA5 reanalysis data between 1979 and 2020. The objectives are as follows: (i) to reconstruct the long-term annual and seasonal B_a on DBG and CSG, (ii) to understand mass wastage-governing energy fluxes at annual and seasonal scale on both the glaciers, and (iii) to quantify the role of sublimation in mass wastage on both the glaciers. Further, the B_a sensitivities for input air temperature, precipitation, and different model parameters are also discussed.

SITE DESCRIPTION, AVAILABLE FIELD MEASUREMENTS, AND CLIMATE DATA

Supplementary Table S1 summarizes the abbreviations, values, units of all variables and parameters used in this study.

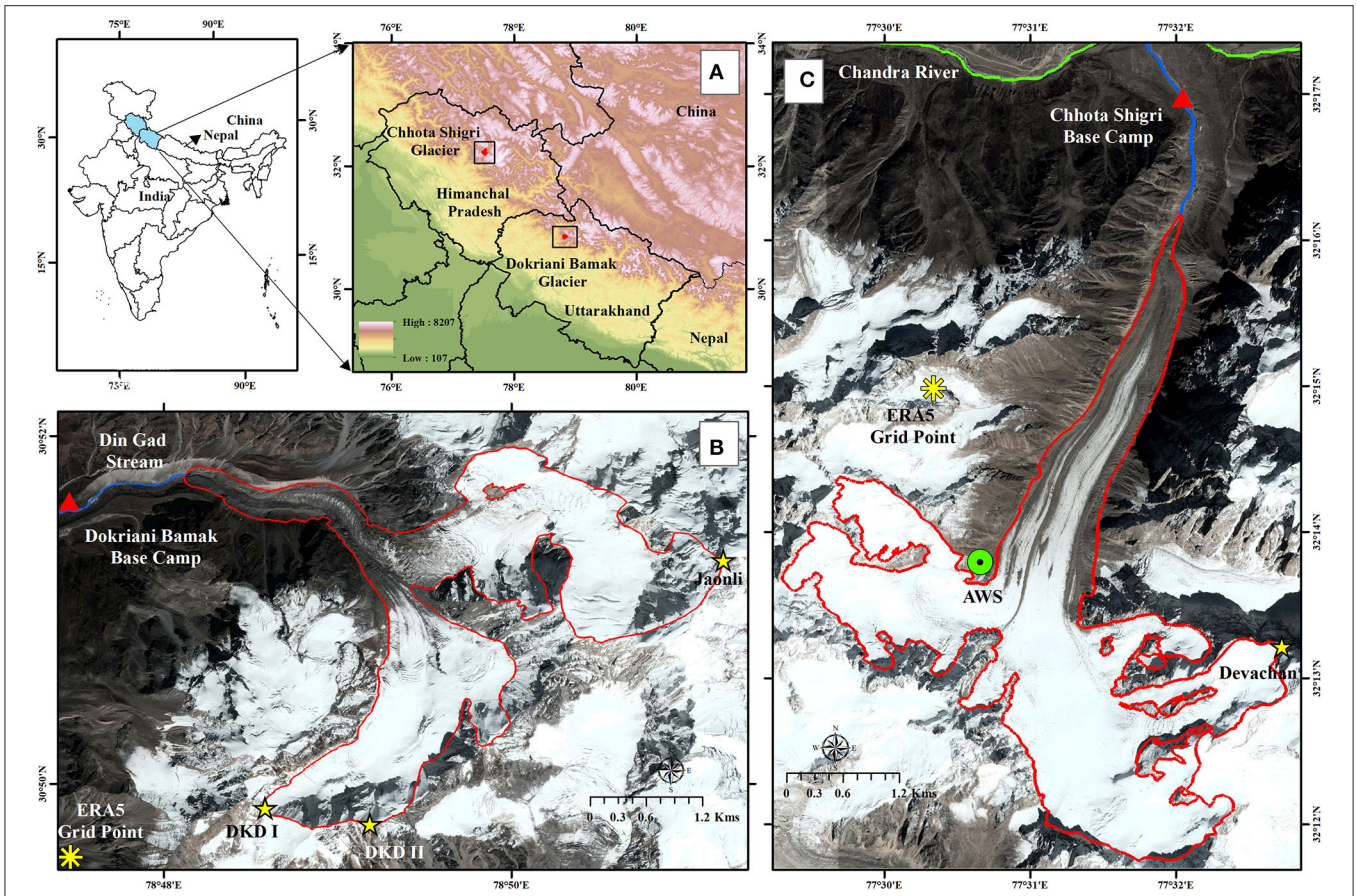

FIGURE 1 | (A) The state boundary of Himanchal Pradesh and Uttarakhand along with locations of Dokriani Bamak and Chhota Shigri glaciers, **(B)** DBG (red outline) on Google earth imagery (CNES-Airbus) of 10 July 2017, and **(C)** CSG (red outline) on Google earth imagery (CNES-Airbus) of 10 April 2017.

Study Area: Dokriani Bamak and Chhota Shigri Glaciers

Dokriani Bamak Glacier (30°51′ N, 78°49′ E) is in the Garhwal range of the central Himalaya (**Figure 1**). It is a valley glacier measuring approximately 6 km in length and an area of 7.03 km^2, and elevation ranging from 4,050 to 6,632 m a.s.l. (**Table 1**) (Azam and Srivastava, 2020). The DBG has a north-west orientation and is guarded by three peaks: Jaonli (6,632 m a.s.l.) in the east, Draupadi Ka Danda I (5,716 m a.s.l.) in the south, and Draupadi Ka Danda II (5,670 m a.s.l.) in the west (**Figure 1**). The DBG tongue (4,050–4,900 m a.s.l.) is partially debris-covered (0.90 km^2, ∼13% of DBG area) (**Figure 1**). The proglacial stream from DBG is called Din Gad which contributes to the Bhagirathi River of the Ganga River system. The DBG has extensively been investigated for its meteorological and mass balance conditions (Verma et al., 2018; Yadav et al., 2019, 2021; Azam and Srivastava, 2020; Dobhal et al., 2021; Garg et al., 2021).

Chhota Shigri Glacier (32°16′ N, 77°34′ E) is in the Lahaul-Spiti valley of the western Himalaya (**Figure 1**). This is a valley glacier with a length of ∼9 km and an area of 15.5 km^2, and elevation ranging from 4,070 to 5,850 m a.s.l. (**Table 1**) (Azam et al., 2016). The CSG is a north-facing glacier, and its upper accumulation area is bounded by valley ridges, with Devachan Peak being the highest (6250 m a.s.l.) point. The terminus of CSG (<4,500 m a.s.l.) is covered with debris (∼4% of CSG area) (Vincent et al., 2013). The CSG drains through a proglacial stream into the Chandra River, a tributary of the Indus River system (**Figure 1**). Since 2002, CSG is under continuous observations focusing on mass balances, SEB, ice thickness-volume-dynamics, and hydrology (Berthier et al., 2007; Wagnon et al., 2007; Soheb et al., 2017; Vashisht et al., 2017; Ramsankaran et al., 2018; Azam et al., 2019; Kumar et al., 2019; Mandal et al., 2020; Haq et al., 2021).

Available Field Data

DBG and CSG have extensively been studied; hence different datasets are available from previous studies. On DBG Base Camp (BC, 3,774 m a.s.l.), an automatic weather station (AWS) logged the data over 2011–2016 while on CSG an AWS, mounted on a side moraine close to high camp (HC, 4,863 m a.s.l.), provided the meteorological data between 2009 and 2017. An automated precipitation gauge (Geonor T-200B) at CSG BC (3,850 m a.s.l.) provided the data since 2012. **Supplementary Table S2** provides the logging details of meteorological data. The locations of AWSs and all-weather precipitation gauge are given in **Figure 1**.

TABLE 1 | List of geographical and topographical characteristics of DBG and CSG.

Glacier characteristics	Dokriani Bamak glacier	Chhota Shigri glacier
Area	7.03 km^2 (2017)	15.5 km^2 (2014)
Debris-covered area	0.94 km^2 (2017)	0.52 km^2 (2014)
Length	∼5 km	∼9 km
Terminus position	4,050 m a.s.l. (2017)	4,072 m a.s.l. (2015)
Orientation	north-west	north
Maximum elevation	6,632 m a.s.l.	5,830 m a.s.l.
Mean mass balance	−0.32 m w.e. (1992–2014)	−0.46 ± 0.40 m w.e. (2002–2019)
Mean ELA*	5,072 m a.s.l. (1992–2013)	5,047 m a.s.l. (2002–2019)
Mean AAR#	67% (1992–2013)	49% (2002–2019)
Mean accumulation area	4.72 km^2	7.5 km^2
Mean ablation area	2.31 km^2	8.0 km^2

ELA, equilibrium line altitude.
#*AAR, accumulation area ratio.*

The measurement of B_a on DBG were conducted intermittently during 1992–2014 (−0.32 m w.e. a^{-1}; 1992–1995, 1996–2000, and 2007–2014) (Dobhal et al., 2021; Garg et al., 2021) while CSG represents the longest continuous B_a series since 2002 (−0.46 ± 0.40 m w.e. a^{-1}) in the Himalaya (Mandal et al., 2020). Altitudinal mass balances (b_a) are also available for 50-m bands over 2009–2013 for DBG (Pratap et al., 2015) and over 2002–2013 for CSG (Azam et al., 2016).

Climate Data and Bias Correction

Daily reanalysis data from ERA5 was used to compute the surface energy fluxes and glacier-wide mass balances on DBG and CSG. ERA5 data is available since 1979 at 0.25° × 0.25° resolution [Copernicus Climate Change Service (C3S), 2017]. The ERA5 data was found to be readily accessible, consistent, and available over a long period, and it has already been used for mass- and energy-balance models in a few studies (Kumar et al., 2021; Patel et al., 2021). Daily incoming shortwave and net radiation (*SWI* and *SWN*), incoming longwave radiation (*LWI*), wind speed (*WS*), relative humidity (*RH*), air temperature (T_a), and precipitation (P) were downloaded for the nearest grids at DBG and CSG (**Figure 1**). The ERA5 raw data series for both the glaciers were bias-corrected using available *in-situ* meteorological data (**Supplementary Table S2**). The bias correction of T_a was done using a linear regression between mean monthly and daily raw ERA5 and *in-situ* T_a data for DBG and CSG, respectively. The bias correction of daily *P*, *WS*, *RH*, *SWI*, *SWN*, and *LWI* were performed using monthly factors derived from monthly *in-situ* and ERA5 raw data on DBG and CSG. *LWI in-situ* data were available from DBG; hence no bias correction was given. All the bias-corrected parameters showed a good coefficient of determination after the bias correction ($R^2 > 0.90$) (**Supplementary Table S2**). The details about the errors before and after bias correction and bias-correction factors are given in the **Supplementary Material** (**Supplementary Figures S1–S13; Supplementary Table S3**).

METHODS

Mass- and Energy-Balance Model

The mass- and energy-balance model (**Figure 2**) computes the SEB fluxes and b_a for each 50-m altitudinal range, and simulates snow accumulation, refreezing of rain/meltwater, surface melt, and sublimation/re-sublimation at daily time step using the long-term, bias-corrected daily ERA5 data between 1979 and 2020 (Section Study Area: Dokriani Bamak and Chhota Shigri Glaciers).

Accumulation Terms

Accumulation terms include solid precipitation and refreezing of rain/melt water at the surface. At a given altitudinal range, the solid precipitation P (mm w.e. d^{-1}) is computed as follows:

$$P = \begin{cases} P: & when \quad T_a \leq T_P \\ 0: & when \quad T_a > T_P \end{cases} \tag{1}$$

Where P and T_a represent daily precipitation (mm) and daily air temperature (°C), respectively, extrapolated at each 50-m altitudinal range, and T_P represents the snow-rain threshold temperature (°C).

Refreezing of rain/melt water at each altitudinal range is computed using Oerlemans 2-m model (Oerlemans, 1992) in which the total energy available for melting (Q_m) is determined by an exponential function of the temperature (θ) of the thermally active layer, considered equivalent to the upper 2-m thickness of a glacier:

$$Q_m = Q\, exp(\theta) \tag{2}$$

$$H_{ice} = Q - Q_m = Q\,[1 - \exp(\theta)] \tag{3}$$

$$c\,\frac{d\theta}{dt} = H_{ice} \qquad \theta \leq 0 \tag{4}$$

Where, Q is the net surface energy budget (W m^{-2}) and H_{ice} is the heat flux generated by refreezing. At the beginning of the mass balance modeling, θ is set to the mean annual T_a, and can only be changed at the beginning of ablation season by refreezing the melt water derived from Equation 4. The value, c is a constant which determines how rapidly the melted snow or ice fraction that runs off reaches 1, and it was set to 1 K^{-1} (Oerlemans, 1992).

Sublimation/re-sublimation (R_s) is calculated using the latent heat flux (*LE)* (Equation 12) and the latent heat of vaporization (l_v, 2.864×10^6 J kg^{-1}) is calculated as follows:

$$R_S = \frac{LE}{l_v} \tag{5}$$

Ablation Terms

The major contribution to glacier ablation comes from the surface melt (Favier et al., 2004; Azam et al., 2014b; Litt et al.,

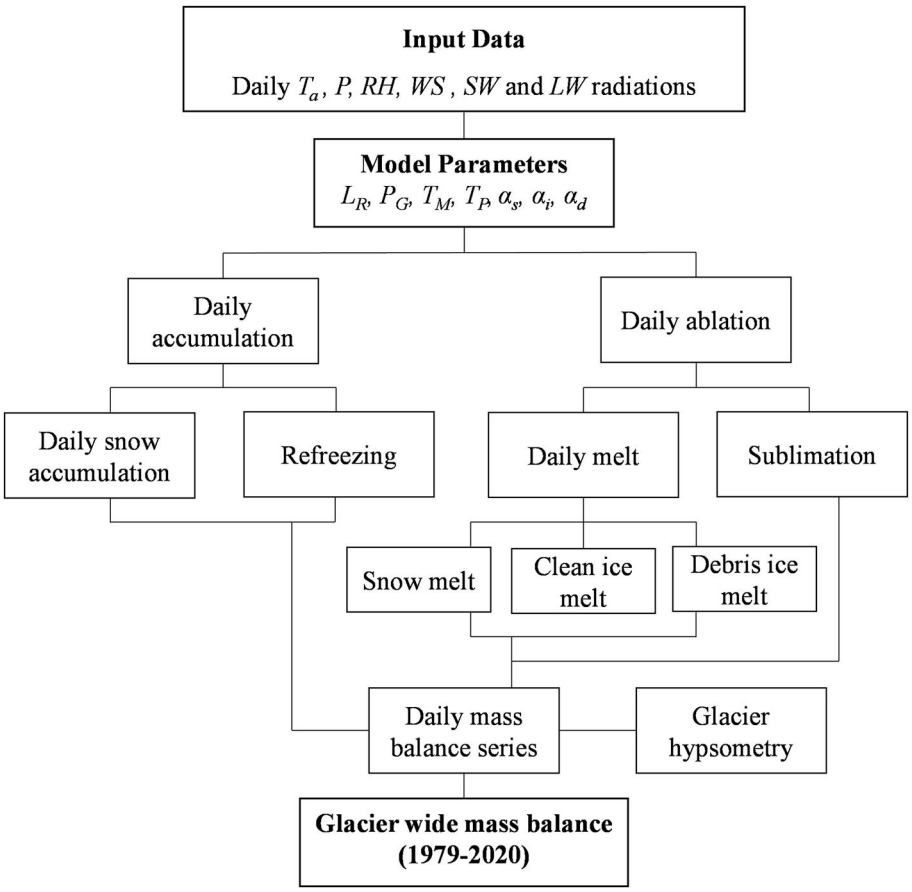

FIGURE 2 | Mass- and energy-balance model structure. T_a is air temperature, P is precipitation, RH is relative humidity, WS is wind speed, SW and LW are the shortwave and longwave radiations, L_R is the temperature lapse rate, P_G is precipitation gradient, T_M is threshold temperature for melt, T_P is threshold temperature for precipitation, α_s is the albedo of snow, α_i is the albedo of ice, and α_d is the albedo of debris cover.

2019) which is calculated using the net energy flux available at the surface. We used a simplified surface energy balance model:

$$Q = \left(1 - \alpha_{s,i,d}\right)\ SWI + LWI - \varepsilon\sigma\ (T_S + 273.15)^4 + H + LE + R \quad (6)$$

Where $\alpha_{s,i,d}$ is the albedo of snow (α_s), ice (α_i), and debris surface (α_d), ε is the emissivity (dimensionless) considered 1, and σ is the Stefan Boltzmann constant $= 5.67 \times 10^{-8}$ W m^{-2} K^{-4}, T_s is the surface temperature (°C). H, LE, and R are the turbulent sensible heat, latent heat, and rain fluxes (W m^{-2}), respectively. Dynamic storage of snow over different altitudinal ranges was maintained using daily accumulation and ablation terms.

Computation of Surface Temperature

Surface temperature (T_S) at each altitudinal range is computed following the calculation of Fujita and Ageta (2000):

$$T_S = T_a + \frac{SWN + \epsilon LWI - \varepsilon\sigma\ (T_a + 273.15)^4 - l_e\rho_a CWS\,(1 - RH)\,q\,(T_a) + H_g}{4\varepsilon\sigma\ (T_a + 273.15)^3 + \left(\frac{dq}{dT_a} l_e + c_a\right)\rho_a CWS} \quad (7)$$

Where, SWN is the net shortwave radiation (W m^{-2}), l_e is the latent heat of evaporation of water (2.5×10^6 J kg^{-1}), ρ_a is the density of air (kg m^{-3}), C is the bulk coefficient (0.002 for snow and clean ice and 0.005 for debris surfaces), $q(T_a)$ is the saturated specific humidity, H_g is the heat transfer into the glacier (W m^{-2}) (here, considered as zero), and c_a is the specific heat of the air (1006 J kg^{-1} K^{-1}). We have considered all the positive surface temperatures which are calculated from Equation 7 as zero because the glacier starts melting if T_a exceeds 0°C.

The value, ρ_a is estimated using the gas equation, where P is the air pressure (P_a) *and* $R_{specific}$ is the specific gas constant for dry air (287.058 J kg^{-1} K^{-1}):

$$\rho_a = \frac{P}{R_{specific}\ T_a} \quad (8)$$

The values, $q(T_a)$ and [$q(T_s)$ in the next Section Computation of Turbulent Heat Fluxes], at a specific temperature, are calculated using the saturation vapor pressure (e^*) at air and surface

temperature, respectively and at air pressure (P) (k Pa):

$$q\left(T_{a,s}\right) = 0.622^{*}\frac{e^{*}}{P} \tag{9}$$

$$e^{*} = 0.611\exp\left(\frac{17.3T_{a,s}}{T_{a,s}+237.2}\right) \tag{10}$$

Computation of Turbulent Heat Fluxes

The values of H, LE, and R are computed using the simplified bulk method (Hay and Fitzharris, 1988):

$$H = c_a\rho_a CWS\left(T_a - T_s\right) \tag{11}$$

$$LE = l_e\rho_a CWS\tau_w[RHq(T_a) - q(T_s)] \tag{12}$$

$$R = c_w\rho_w w(T_r - T_s) \tag{13}$$

Where, c_w is the specific heat of water (4,200 J kg^{-1} K^{-1}), ρ_w is the density of water (kg m^{-3}), T_r is the rainfall temperature (assumed equal to be T_a), w is the rainfall rate (m s^{-1}), τ_w is the wetness parameter whose value is considered 1 for snow and ice surfaces, but it varies over the debris-covered surface (**Supplementary Section 2**). In the present study, we used the bulk method for the calculation of energy fluxes which is known to give reasonable results even in katabatic winds conditions (Denby and Greuell, 2000).

Computation of Mass Balance

The surface melt is calculated using the heat available for melting at different surfaces [$Q_{(s,i,d)}$, W m^{-2}]. The net energy available at the surface is used to produce the melt when T_s is above the threshold temperature for melt (T_M); otherwise, it is used to raise the T_s up to T_M:

$$M\left(s,i,d\right) = \begin{cases} 0: & when \quad T_s \le T_M \\ Q_{\frac{(s,i,d)}{l_m}}: & when \quad T_s > T_M \end{cases} \tag{14}$$

where l_m is the latent heat of fusion (3.33×10^5 J kg^{-1}) and $Q_{(s,i,d)}$ is the amount of total energy available at the different surfaces.

The value, b_a for each 50-m altitudinal range (m w.e.) is estimated using the accumulation and the ablation terms as follows:

$$b_a = \frac{(P_S + R_F) - \left(M(s,i,d) - R_S\right)}{\rho_w} \tag{15}$$

Where ρ_w is the density of water (1,000 kg m^{-3}).

B_a, (m w.e.) is calculated using the mean b_a:

$$B_a = \frac{\sum A_a b_a}{A} \tag{16}$$

Where, A_a (m^2) and b_a (m w.e.) are the 50-m altitudinal glacier area and mean mass balance, respectively, and A is the total glacier area (m^2). The value, B_a is calculated using daily values for the hydrological year from 1 November through 31 October of the next year for the DBG (Dobhal et al., 2008) and hydrological year from 1 October through 30 September of the next year for the CSG (Wagnon et al., 2007). The overall structure of the model is given in **Figure 2**.

Model Parameters

In the mass-, and energy-balance model, T_a is one of the most important parameters, as it decides the precipitation phase (snowfall or rain) (Hock, 2003; Shea et al., 2015a). In this study we calculated the extrapolated values of T_a using the temperature lapse rates (T_{LR}) developed using field observations (Azam et al., 2014a; Azam and Srivastava, 2020). Further, the T_p values were adopted from Jennings et al. (2018), where we used a T_p value of 0.7° and 1.1°C corresponding to 70–80% and 60–70% RH ranges for DBG and CSG, respectively, at which 90–100% precipitation was considered as snow.

The net solar radiation is also crucial in the surface mass, and energy-balance modeling, and the amount of insolation available for melt production largely depends on surface albedo (Azam et al., 2014b; Litt et al., 2019). Surface albedo values (α_s, α_i, and α_d) have high spatiotemporal variability over the glaciers. Deposition of dust and black carbon aerosols together with progressive snow metamorphism and compaction makes albedo values very uncertain (Oerlemans and Knap, 1998; Brock and Arnold, 2000). Moreover, the mass, and energy-balance models are highly sensitive to surface albedo (Kayastha et al., 1999; Acharya and Kayastha, 2019; Johnson and Rupper, 2020; Stigter et al., 2021); therefore, surface albedo values (α_s, α_i, α_d) are calibrated in the present study using the plausible ranges available from the study of Cuffey and Paterson (2010). Due to lack of information related to surface albedo evolution in the study area as well as to keep the model computationally simple, we have used static but separate calibrated albedo values for snow, ice, and debris surfaces, as also adopted in some other previous studies (Ragettli et al., 2013, 2015; Acharya and Kayastha, 2019). Energy, and mass-balance models are also sensitive to T_M, often unknown in the HK (Engelhardt et al., 2017; Azam et al., 2019; Azam and Srivastava, 2020). Further, the distribution of precipitation over glaciers is one of the biggest challenges in glaciological modeling, and it is spatially non-uniform in the HK region due to valley-specific precipitation gradients (P_G) (Maussion et al., 2014; Immerzeel et al., 2015; Sakai et al., 2015). Given that T_M, P_G, α_s, α_i, and α_d are highly sensitive parameters and least explored in the HK region; therefore, they are used for the calibration of the mass- and energy-balance model in this study.

Model Calibration

For the calibration of the mass- and energy-balance model, Monte Carlo simulations are performed with 10,000 parameter sets where the parameters are varied over their plausible limits (Konz and Seibert, 2010; Rounce et al., 2020). The value, P_G is changed from 0 to 100% km^{-1}, T_M from −3°C to +3°C, α_s from

TABLE 2 | List of model parameters, sensitivity and uncertainty ranges for DBG and CSG.

Parameters	Dokriani Bamak glacier				Chhota Shigri glacier			
	Model value	Uncertainty estimation range	Sensitivity test range	Mass balance sensitivity (m w.e. a^{-1})	Model value	Uncertainty estimation range	Sensitivity test range	Mass balance sensitivity (m w.e. a^{-1})
Altitudinal precipitation gradient (% km^{-1})*	36	33 to 40	33 to 40	0.08	73	66 to 81	66 to 81	0.06
Temperature Lapse rate (T_{LR}) (°C km^{-1})	$T^{\#}_{LR}$	L_R+1σ to L_R-1σ	L_R+1σ to L_R-1σ	0.10	$T^{\$}_{LR}$	L_R+1σ to L_R-1σ	L_R+1σ to L_R-1σ	0.12
Threshold temperature for snow/rain (T_P) (°C)	0.70	0.63 to 0.77	0.60 to 0.80	0.02	1.10	0.99 to 1.21	1 to 1.20	0.01
Threshold temperature for melting (T_M) (°C)*	−1.90	−1.71 to −2.09	−1.71 to −2.09	0.01	−1.83	−1.65 to −2.01	−1.93 to −1.73	0.02
Albedo of snow (α_s) *	0.77	0.69 to 0.85	0.69 to 0.85	0.29	0.77	0.70 to 0.84	0.70 to 0.84	0.37
Albedo of clean ice (α_i)*	0.47	0.42 to 0.51	0.42 to 0.51	0.02	0.50	0.36 to 0.44	0.36 to 0.44	0.02
Albedo of Debris-covered ice (α_d)*	0.16	0.14 to 0.18	0.14 to 0.18	0.02	0.13	0.13 to 0.15	0.13 to 0.15	0.001
Temperature (1°C)	–	–	T+1 to T−1	−0.50	–	–	T+1 to T−1	−0.30
Precipitation (10%)	–	–	−10% to +10%	0.23	–	–	−10% to +10%	0.13

**Calibrated parameters; #Monthly lapse rate; $Daily lapse rate.*

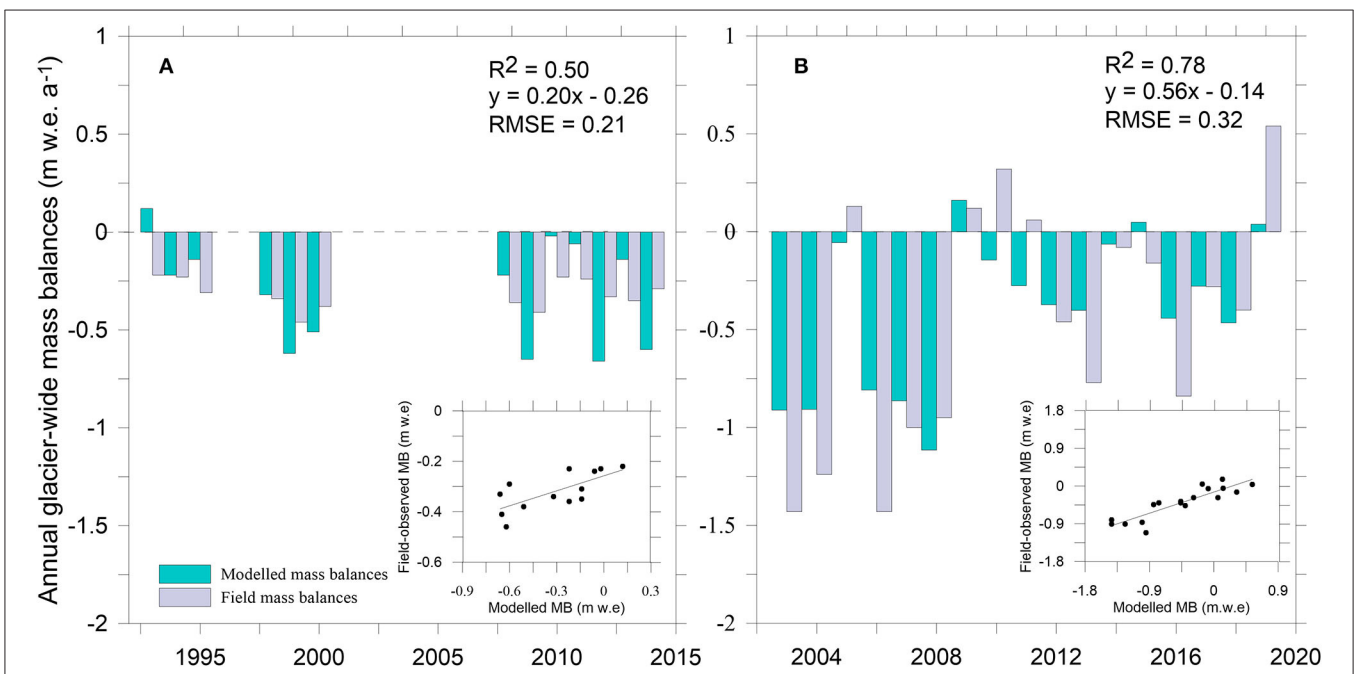

FIGURE 3 | Model calibration: the modeled (green) and *in-situ* (violet) B_a on DBG over 1992-2014 **(A)**, and CSG over 2003–2019 **(B)**. Insets in both the panels show the correlations between modeled and *in-situ* mass balances.

0.45 to 0.85, α_i from 0.35 to 0.55, and $\alpha_d$from 0.1 to 0.2 following the study by Cuffey and Paterson (2010). The runs with minimum RMSE between modeled and *in-situ* B_a are selected for both the glaciers. The selected runs show an RMSE of 0.21 m w.e. a^{-1} (1992–2014) and 0.32 m w.e. a^{-1} (2002–2019) between modeled and *in-situ* B_a for DBG and CSG, respectively. The difference between the modeled and *in-situ* mean B_a are 0.01 and 0.06 m w.e. a^{-1} on DBG and CSG, respectively (**Table 2**; **Figure 3**).

Model Validation

Altitudinal Mass Balances

The model is validated against the *in-situ* mean b_a available for 50-m bands from 4,050 to 4,950 m a.s.l. over 2009–2013 for DBG and from 4,250 to 5,300 m a.s.l. over 2002–2013 for CSG (Section Available Field Data). The agreement between modeled and *in-situ* b_a shows a good agreement with R^2 of 0.88 and 0.98 over clean ice on DBG and CSG, respectively

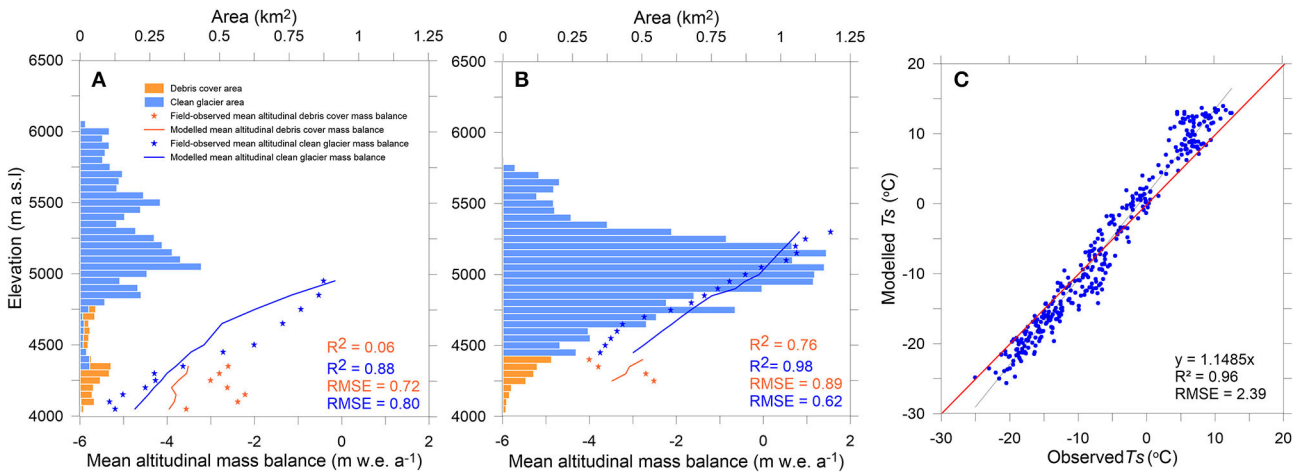

FIGURE 4 | Model validation: the modeled and *in-situ* mean b_a over 2009–2013 for DBG **(A)**, over 2002–2013 for CSG **(B)**, and surface temperature **(C)** [In **(A,B)**, orange and blue bars show the 50-m hypsometry of debris-covered and clean glacier; orange and blue stars show the *in-situ* mean b_a for the debris-covered and clean glacier; orange and blue lines show the modeled mean b_a for the debris-covered and clean glacier].

(**Figures 4A,B**). Conversely but expectedly, this agreement over debris cover is very poor on both the glaciers. This is due to the strong spatial variability in debris distribution on both the glaciers that results in strong heterogeneous melt over the debris cover area (Vincent et al., 2013; Pratap et al., 2015). The *in-situ* b_a at each altitudinal range were estimated by taking a single stake data or the mean of a couple of stakes inserted at selected flat locations having moderate (5–40 cm) debris thickness (avoiding very thick debris) on both the glaciers (Wagnon et al., 2007; Pratap et al., 2015); hence the estimated b_a does not represent the whole 50-m altitudinal range. The debris-cover area (DBG = ∼13%; CSG = ∼4%) and the melt contribution (DBG = 17%; CSG = 6%) on both the glaciers is limited; therefore, the impact of possible mismatch between modeled and observed b_a over debris cover on B_a can be assumed small. This assumption is also supported by the negligible modeled B_a sensitivity to α_d on both the glaciers (Section Annual Glacier-Wide Mass Balance Sensitivity; **Table 2**). Though the comparison of modeled b_a with *in-situ* data over debris cover serves no purpose, it echoes the limitation of conventional glaciological method for mass balance estimation over debris cover area (Azam et al., 2018).

Surface Temperature

Surface energy balance models are very sensitive to T_s; thus, another validation is performed for T_s. The modeled daily T_s (Section Computation of Surface Temperature) are compared with the observed T_s, derived from the bias-corrected *LWO* at CSG AWS. A good agreement between the modeled and observed T_s (R^2 = 0.96; 14.85% overestimation, **Figure 4C**) indicates the robustness of the surface temperature scheme. The *in-situ LWO* data are not available for DBG; hence a similar validation could not be performed there. These validations of the model output against the observed b_a (**Figures 4A,B**) and observed T_s (**Figure 4C**) suggest that the model is robust enough to reconstruct the mass balances.

Uncertainty Estimation

The model parameters are the key source of uncertainty in the modeled mass balances (Ragettli et al., 2013; Shea et al., 2015b). Parametric uncertainties are calculated by re-running the model while adjusting the parameters one-by-one within a reasonable range of their calibrated values and keeping the other model parameters unchanged (**Table 2**). The uncertainties in T_{LR} are taken as standard deviations of mean monthly values for both DBG and CSG. The uncertainties in other parameters (α_s, α_i, α_d, P_G, T_M and T_P) are unknown; hence these parameters are varied with the range of ±10% from their calibrated values (Anslow et al., 2008; Ragettli et al., 2013, 2015).

The total uncertainty in B_a is calculated by summing up all parametric uncertainties by applying the error propagation rule. The estimated mean uncertainties for B_a are 0.32 m w.e a^{-1} and 0.38 m w.e a^{-1} for DBG and CSG, respectively over 1979–2020. Among all the parameters, the highest uncertainty in B_a on both the glaciers is contributed by α_s (**Table 2**). The parametric uncertainty in the summer and winter mass balances are 0.38 and 0.01 m w.e a^{-1} for DBG and 0.36 and 0.02 m w.e. a^{-1} for CSG, respectively over 1979–2020.

In this study, a fixed glacier hypsometry was used on both the glaciers. For DBG, the hypsometry was manually delineated from high-resolution CNES-Airbus data from 10 July 2017 using a high-resolution Google Earth platform (Azam and Srivastava, 2020) while hypsometry for CSG was estimated using a digital elevation model (DEM) developed using Pléiades stereo pair from 18 August 2014 (Azam et al., 2016). This fixed area assumption introduces uncertainties to the modeled B_a, but these were found to be insignificant comparing the total estimated uncertainty in B_a in previous studies using T-index models (Azam et al., 2019; Azam and Srivastava, 2020), and hence they are ignored in this present study.

RESULTS

Meteorological Conditions and Seasonal Characteristics

The HK Mountain range is located in the sub-tropical climate zone with a large annual temperature amplitude resulting in clear summer and winter seasons. The climate of HK is controlled by the Indian winter monsoon (IWM), embedding western disturbances, mainly during winters and the Indian summer monsoon (ISM), mainly during the summer (Gadgil et al., 2003; Dimri et al., 2016). The influence of IWM decreases eastwards; conversely, the intensity of the ISM decreases westwards along with the HK mountain range (Maussion et al., 2014). *In-situ* meteorological data from DBG and CSG are available for short periods (Section Available Field Data); therefore, long-term, bias-corrected ERA5 data over 1979–2020 are exploited to understand the mean seasonal characteristics on both the glaciers.

Mean monthly cycles of T_a and RH on both the glaciers followed roughly similar trends; however, the WS showed strong seasonality on DBG and moderate winds on CSG (**Figure 5**). The amplitudes of mean monthly T_a and RH ($T_{aDBG} = -7.2°C$ and $RH_{DBG} = 46\%$ on DBG and $T_{aCSG} = -6.1°C$ and $RH_{CSG} = 47\%$ on CSG) were sufficiently large to characterize the different seasons. A humid, warm, and less windy summer-monsoon from June through September and a less humid, cold, and windy winter season from December through March were demarcated on both the glaciers (**Figure 5**). A pre-monsoon over April–May and a post-monsoon over October–November were also defined (**Supplementary Table S4**). The same season demarcation was suggested on CSG by Azam et al. (2014a) using 3-years of AWS data (**Figure 1**).

The summer-monsoon was the warmest ($T_{aDBG} = -1.5°C$, $T_{aCSG} = 1.8°C$), least windy ($WS_{DG} = 3.6\ m\ s^{-1}$, $WS_{CSG} = 4.8\ m\ s^{-1}$), and the most humid ($RH_{DBG} = 63\%$, $RH_{CSG} = 61\%$) season of both the glaciers (**Supplementary Table S4**). Conversely, the winter season was the coldest, much below the freezing point ($T_{aDBG} = -12.7°C$, $T_{aCSG} = -13.5°C$), and windiest ($WS_{DBG} = 8.8\ m\ s^{-1}$, $WS_{CSG} = 5.7\ m\ s^{-1}$) on both the glaciers. Pre-monsoon and post-monsoon showed the moderate conditions for T_a, RH, and WS (**Supplementary Table S4**). Modeled surface temperature (T_s) was always negative on both the glaciers except for the summer-monsoon when it was close to 0°C, showing the melting at the surface due to higher T_a of the summer monsoon (**Supplementary Table S4**).

The mean monthly P cycles were remarkably different on both the glaciers (**Figure 5**). The ISM brought the major amount of annual P (74%) over DBG during the summer monsoon, while IWM brought the major amount of annual P (53%) over CSG during the winter. Therefore, these glaciers can be considered as summer accumulation-type and winter accumulation-type glaciers, respectively. The mean annual P on DBG was almost double that of CSG (**Supplementary Table S4**). Systematically, P amounts on DBG in all seasons were 1.5–2 times less than that of CSG except the summer monsoon when P on DBG was 9 times compared to CSG (**Supplementary Table S4**).

Despite the maximum solar angle in the summer monsoon, SWI was maximum during pre-monsoon on both the glaciers ($SWI_{DBG} = 298\ W\ m^{-2}$, $SWI_{CSG} = 418\ W\ m^{-2}$) because monsoonal cloud cover impedes the SWI in the summer monsoon (Azam et al., 2014b; Litt et al., 2019). However, this effect was much stronger on DBG due to strong monsoonal influence (**Figure 5**). The reduced SWI ($SWI_{DBG} = 294\ W\ m^{-2}$, $SWI_{CSG} = 410\ W\ m^{-2}$) during the summer monsoon was compensated by the highest LWI ($LWI_{DBG} = 310\ W\ m^{-2}$, $LWI_{CSG} = 272\ W\ m^{-2}$) on both the glaciers—mostly emitted from warm, dense summer-monsoonal clouds, and surrounding valley walls. Post-monsoon and winter exhibited quite similar conditions, receiving lower SWI and LWI due to decreasing solar angle, T_a, and RH (**Supplementary Table S4**).

Glacier-Wide Annual and Seasonal Mass Balances

The modeled mass wastage was moderate and similar on both the glaciers with a mean wastage of -0.27 ± 0.32 m w.e. a^{-1} (equivalent cumulative mass wastage of -11.16 ± 2.06 m w.e.) on DBG and -0.31 ± 0.38 m w.e. a^{-1} (equivalent cumulative mass wastage of -12.61 ± 2.67 m w.e.) on CSG, over 1979–2020 (**Figure 6**). The years 1982/83 and 1988/89 showed the maximum B_a of 0.20 ± 0.33 m w.e. and 0.42 ± 0.23 m w.e., while the year 2000/01 showed the minimum B_a of -0.75 ± 0.32 m w.e. and -1.49 ± 0.76 m w.e. for DBG and CSG, respectively. The value of B_a was negative for 35 and 27 years and positive for 6 and 14 years on DBG and CSG, respectively. Though the mean mass wastage on both the glaciers was almost the same, the mass turnover on CSG (1.27 m w.e. a^{-1}) was higher than that of DBG (0.92 m w.e. a^{-1}) (**Figure 6**). This is due to the fact that CSG is a winter accumulation-type glacier and receives a lot of accumulation during winter and is melted out during the summer-monsoon, while for DBG, the accumulation and ablation seasons coincide during the summer monsoon (Section Meteorological Conditions and Seasonal Characteristics).

Modeled seasonal mass balances ranged from 0.07 to 0.69 m w.e. a^{-1} and 0.17 to 0.72 m w.e. a^{-1} for winter, and -1.00 to -0.16 and -1.69 to -0.06 w.e. a^{-1} for summer on DBG and CSG, respectively. The mean summer and winter mass balances were -0.60 ± 0.30 and 0.32 ± 0.02 m w.e. a^{-1} on DBG and -0.79 ± 0.36 and 0.48 ± 0.02 m w.e. a^{-1} on CSG for the period 1979–2020, respectively.

Seasonal and Annual Glacier-Wide Surface Energy Balance

Surface energy balance mainly depends on the seasons (Litt et al., 2019). In the summer-monsoon, SWN was the highest with mean values of 100 and 125 W m^{-2} on DBG and CSG, respectively, with high daily variability from 71 to 151 W m^{-2} and 76 to 171 W m^{-2}, respectively (**Figure 7**). The LWN was also maximum, with mean values of -4 and -41 W m^{-2} on DBG and CSG, respectively, in the summer monsoon due to humid, warm, and dense cloud cover conditions that result in high values of LWI (**Supplementary Tables S4, S5**). Highest SWN and LWN resulted in the highest net radiation (R_n) at the surface during the summer monsoon with the mean seasonal values of 95 and 84 W m^{-2} on DBG and CSG, respectively

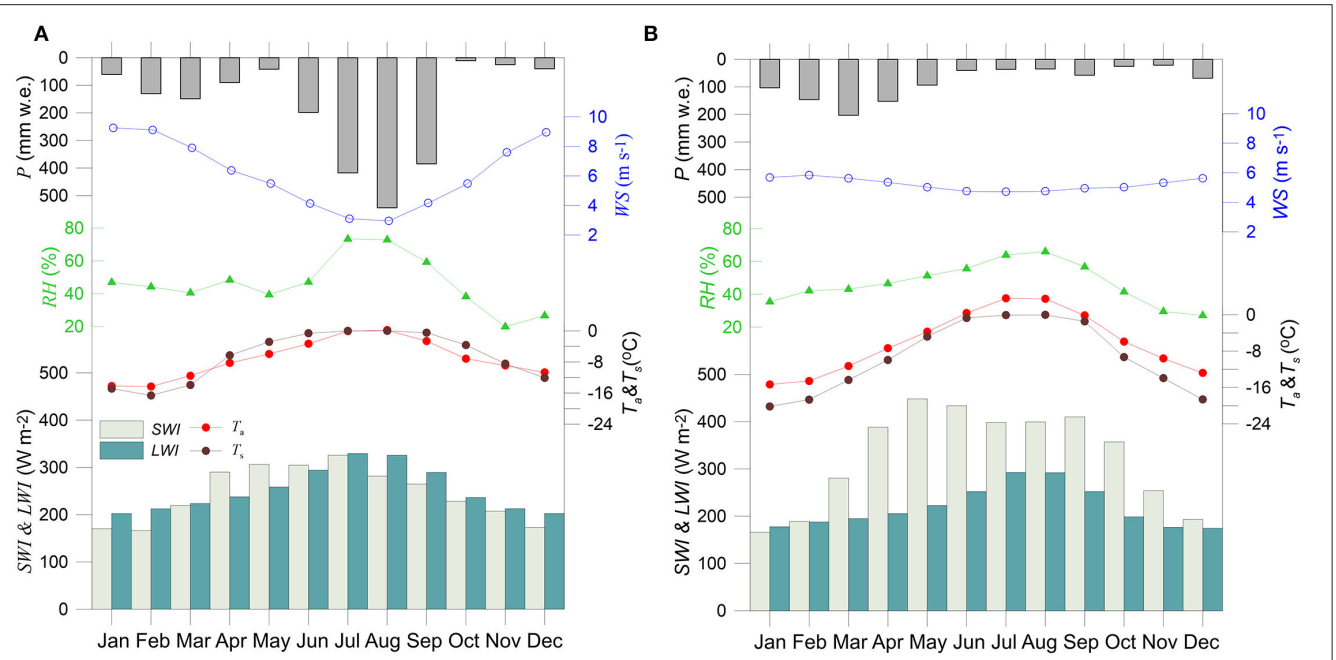

FIGURE 5 | Glacier-wide mean monthly values of T_a (red dots), T_s (brown dots), *RH* (green triangles), *WS* (blue circles), *P* (gray bars), *SWI* (orange bars) and *LWI* (violet bars) at **(A)** DBG base camp (3,774 m a.s.l.) and **(B)** CSG high camp (4,863 m a.s.l.), respectively from bias-corrected ERA5 data over 1979–2020. *SWI* and *LWI* are at point scale while all other parameters are at glacier-wide scale.

(**Figure 7**; **Supplementary Table S5**). Both the glaciers gained a small amount of energy through *H*. Conversely, a small amount of energy was released through *LE*—indicating some mass loss through sublimation (**Supplementary Table S5**). The resulting energy, *Q*, was the highest and positive during the summer monsoon on both the glaciers mainly due to the highest values of both *SWN* and *LWN* (**Supplementary Table S5**).

In winter, *SWN* was the least with 42 and 37 W m^{-2} values while *LWN* remained moderate with −45 and −57 W m^{-2} values on DBG and CSG, respectively (**Supplementary Table S5**). Winter *SWN* and *LWN* showed comparatively less variability on both the glaciers (**Figure 7**). In winter, DBG and CSG released some energy (−3 and −20 W m^{-2}, respectively) through R_n (**Figure 7**). Like CSG, a recent study also found negative R_n during winter on 8 glaciers in the Chandra valley, including CSG (Patel et al., 2021). Due to the higher temperature gradient and strongest *WS* in winter (**Supplementary Table S4**), *H* was the maximum and provided 13 and 23 W m^{-2} energy at the surface of DBG and CSG, respectively (**Supplementary Table S5**). The *LE* was moderately negative during winter showing moderate glacier-wide sublimation (**Supplementary Table S5**). The net energy, *Q*, was also moderate but negative with −23 and −16 W m^{-2} values, mainly due to the least values of winter *SWN* on both the glaciers (**Supplementary Table S5**).

In pre-monsoon and post-monsoon, the *SWN* values were moderate as 67 and 56 W m^{-2} on DBG, and 87 and 61 W m^{-2} on CSG, respectively (**Supplementary Table S5**). Energy loss through *LWN* was the highest in post-monsoon when compared to other seasons on both the glaciers (**Figure 7**). The value R_n was positive in pre-monsoon while negative in post-monsoon (**Supplementary Table S5**) due to the most negative *LWN* values in post-monsoon on both the glaciers. Both DBG and CSG gained more energy in the form of *H* in post-monsoon than in pre-monsoon (**Figure 7**). The most negative values of *LE* in pre-monsoon and post-monsoon (**Supplementary Table S5**) indicate the maximum mass loss through sublimation during these seasons. The *Q* value was the least in both pre-monsoon and post-monsoon due to higher negative values of *LWN* and *LE*, and moderate values of *SWN* (**Supplementary Table S5**).

Similar to previous studies on the HK region (Mölg et al., 2012; Azam et al., 2014b; Huintjes et al., 2015a,b; Johnson and Rupper, 2020; Patel et al., 2021), annual glacier-wide *SWN* contributed the maximum amount of energy to the total SEB on DBG and CSG. Further, both the glaciers lost energy through *LWN* at −35 and −57 W m^{-2}, respectively. The value of *H* brought some energy throughout the year with 9 and 15 W m^{-2} values on DBG and CSG, respectively (**Supplementary Table S5**; **Figure 7**). Patel et al. (2021) also observed a similar mean annual value of *H* on 8 glaciers in the Chandra valley (**Figure 7**). *LE* remained negative throughout the year on both the glaciers indicating mass loss through sublimation, in line with other glacier-wide SEB studies in the HK region (Huintjes et al., 2015a,b; Patel et al., 2021). Annually, the highest *SWN* results in maximum R_n followed by *H* and *LE* on both the glaciers. Annual glacier-wide net energy, *Q*, was positive with a value of 10 W m^{-2} on both DBG and CSG (**Supplementary Table S5**), indicating a net

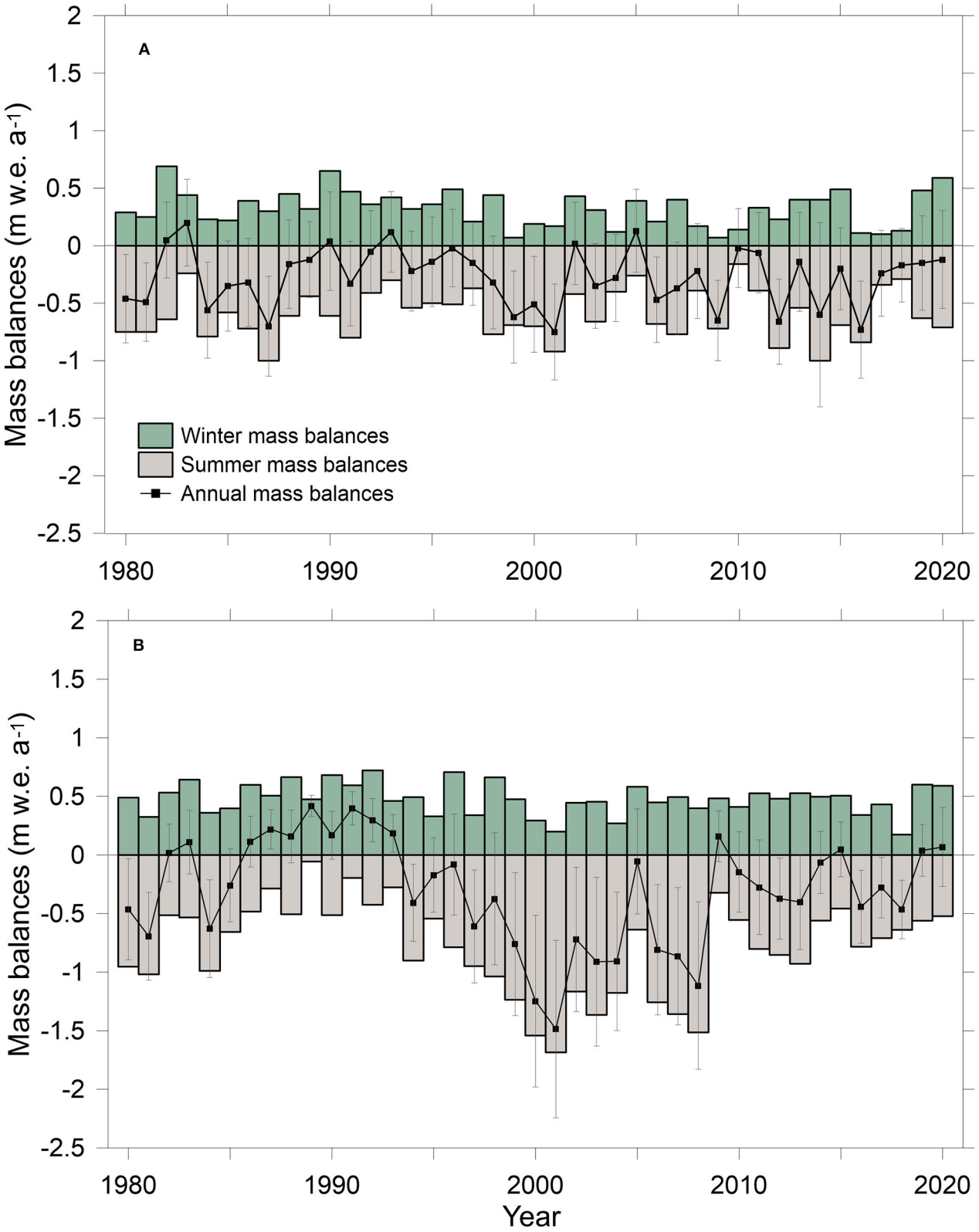

FIGURE 6 | Annual mass balances (black squares), winter mass balances (green bars), and summer mass balances (gray bars) over 1979-2020 on **(A)** DBG and **(B)** CSG, respectively. The uncertainties of annual mass balances are shown.

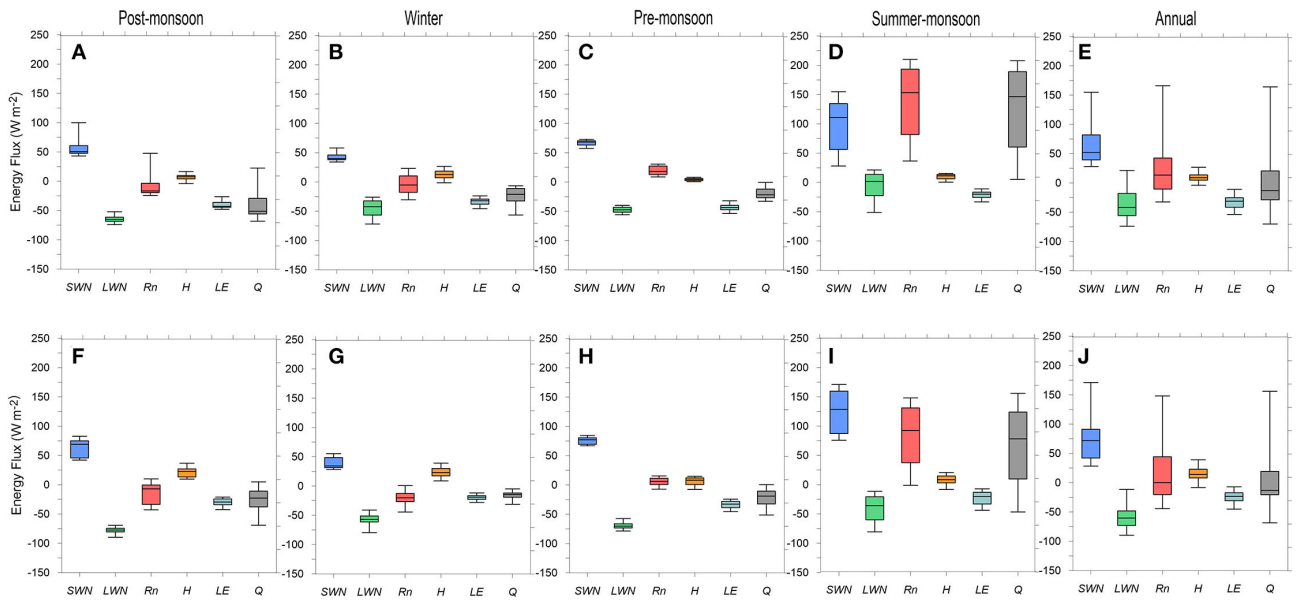

FIGURE 7 | Box-whisker plots of mean daily SEB components calculated from all available data from 1979-2020 and classified into seasons, post-monsoon, winter, pre-monsoon, and summer-monsoon. The boundaries of each box cover the 25th to the 75th percentile of each distribution, while the middle line of the box shows the median value. Box-whisker in **(A–E)** shows the values for DBG and **(F–J)** CSG, respectively.

glacier-wide wastage (Section Glacier-Wide Annual and Seasonal Mass Balances).

Altitudinal Distribution of Mean Annual Mass Balance and SEB

The mean 50-m b_a varied from −4.62 to 2.20 m w.e. on DBG and −1.95 to 0.57 m w.e on CSG (**Figure 8**). On DBG, the terminus area less than 4,950 m a.s.l. showed less glacier wastage toward the valley walls compared to the middle of the glacier (**Figure 8**). This is due to the distribution of debris cover on DBG which is thicker toward valley walls (Pratap et al., 2015). Similarly, the CSG terminus area less than 4,400 m a.s.l. also showed less mass wastage (**Figure 8**) due to thick debris cover (Vincent et al., 2013). Despite the lowest albedo of debris cover which results in the highest *SWN* over the debris-covered glacier with mean values of 188 and 141 W m^{-2} on DBG and CSG, respectively, the melting was the least due to a thick debris cover that protects the glacier from higher melt (Vincent et al., 2016; Banerjee, 2017). Going up on the glacier, the b_a increased and becomes positive in the accumulation areas on both the glaciers (**Figure 8**). The increase in b_a with altitude closely followed *SWN* which continuously reduced with altitude and achieved near-constant values of 56 and 59 W m^{-2} at higher altitudes on DBG (>5,250 m a.s.l.) and CSG (>5,050 m a.s.l.) glaciers, respectively. This was probably due to the permanent snow cover in the accumulation area, having higher surface albedo values near stable *SWN*. Glaciers lost some energy through *LWN* which was highly negative over lower reaches (<4,500 m a.s.l.) compared to higher altitudes on both the glaciers (**Figure 8**). The value of R_n was higher over lower reaches (<4,850 m a.s.l.), and showed a reduction between 4,800 to 5,500 m a.s.l. and again increased slightly toward higher reaches (>5,500 m a.s.l.) due to the highest *LWN* at higher reaches on both the glaciers (**Figure 8**). The DBG showed high and positive *H* values at lower altitudes (<5,250 m a.s.l.) and slightly negative values at higher altitudes due to the negative air-surface temperature gradient (T_a – T_s) while it remained positive over the whole CSG (**Figure 8**). The *LE*, generally more negative at higher altitudes, showed altitudinal mass loss through sublimation equivalent to −6 to −42 W m^{-2} on both DBG and CSG (**Figure 8**). The resulting energy, *Q*, was positive at lower altitudes (<5,000 m a.s.l.) and became negative at higher altitudes on both the glaciers (**Figure 8**).

On the DBG terminus area (<4,950 m a.s.l.), all the SEB components showed different behaviors toward valley walls as compared to the middle of the glacier due to the thick debris cover over the valley walls (**Figure 8**). Due to the low albedo of debris cover, *SWN* was the highest that resulted in maximum R_n and *Q* over those areas (**Figure 8**). *H* was slightly negative over debris-covered area compared to positive values at the middle of the glacier while *LE* was slightly less negative over the debris-covered area compared to more negative values at the middle of the glacier. This is due to the higher T_s than T_a over the debris-covered area due to the unavailability of snow or ice cover mainly during the summer-monsoon (**Figure 8**).

Glacier-Wide Sublimation

The mean glacier-wide sublimation was computed as −1.28 and −0.66 mm w.e. d^{-1} over 1979–2020, with a strong spatial and temporal variability, on DBG and CSG, respectively (**Figures 8**, **9**). The mean monthly sublimation was higher in May on both DBG (−1.93 mm w.e. d^{-1}) and CSG (−1.06 mm w.e. d^{-1}) glaciers, and sharply decreased over July–August as soon as

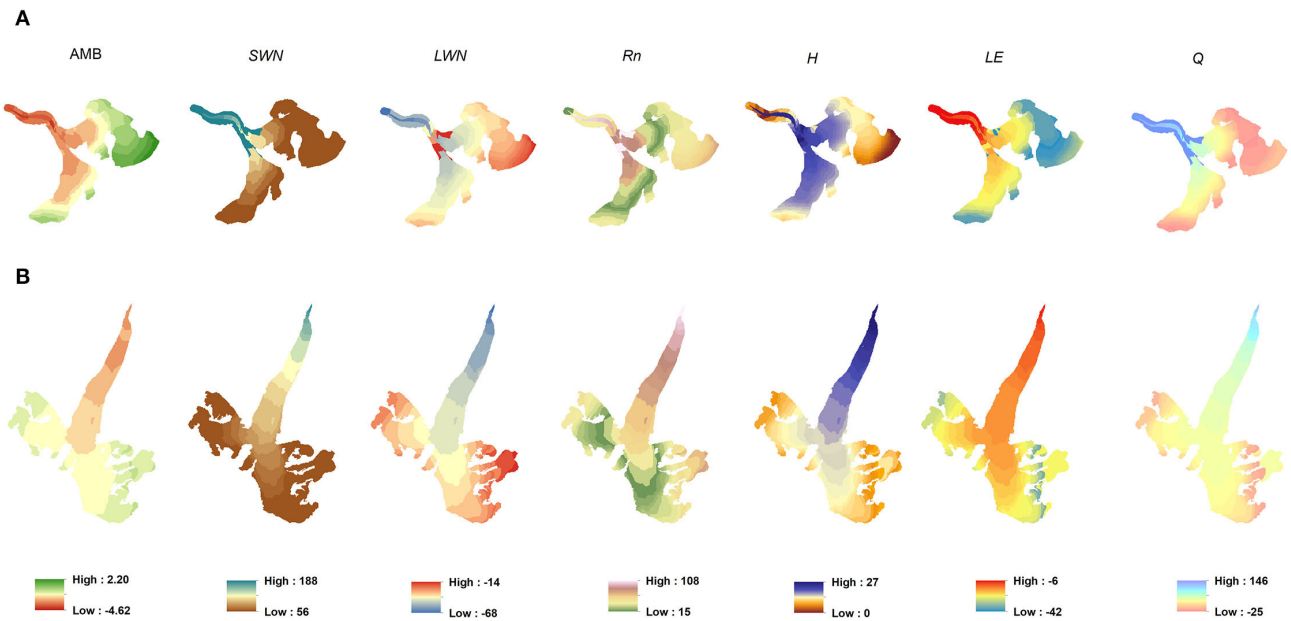

FIGURE 8 | Distribution of modeled mean altitudinal mass balances and mean SEB components for 1979–2020 period of **(A)** DBG and **(B)** CSG, respectively (DBG and CSG are not in same scale).

monsoon arrived over these glaciers (**Figure 9**). Despite the lowest *WS*, the highest *RH* and T_a in the summer-monsoon months (**Figure 9**) reversed the specific humidity gradient. This reversal led to slightly positive values of *LE*, at least over the ablation area, in July–August indicating re-sublimation on both the glaciers (Section SEB in Ablation and Accumulation Zones). This provided the least glacier-wide values of *LE* and the least amounts of sublimation in the summer-monsoon on both the glaciers (**Figure 9**). The sign reversal of *LE* from the negative to positive values during humid and warmer conditions has also been observed from SEB studies on different mountain ranges, including the HK region (Wagnon et al., 1999, 2003; Oerlemans, 2000; Sicart et al., 2005; Azam et al., 2014b; Stigter et al., 2018; Litt et al., 2019). Even though the *WS* was the highest in winter, the mean monthly glacier-wide sublimations were moderate due to the lowest *RH* and T_a on both the glaciers, whereas sublimation was the highest during pre-monsoon and post-monsoon months corresponding to moderate *WS, RH*, and T_a (**Figure 9**). The computed glacier-wide sublimation losses account for significant amounts of 22 and 20% of total ablation on DBG and CSG, respectively; therefore, we stress that the inclusion of a simplified sublimation scheme in mass balance modeling using T-index models, have not yet included. Simplified scheme may parametrize the sublimation as a function of temperature, humidity, and wind speed (Azam et al., 2021).

Relative Mass Wastage From Snow, Clean Ice, and Debris-Covered Ice

Snow, clean ice, and debris-covered ice ablation contributed 56, 27, and 17% to the total ablation on DBG, while on CSG, these contributions were 65, 29, and 6%, respectively. In agreement to the highest glacier-wide snow ablation over both the glaciers, previous glacio-hydrological T-index modeling studies also suggested that the snowmelt contribution was the maximum on DBG and CSG (Engelhardt et al., 2017; Azam et al., 2019; Azam and Srivastava, 2020). A slightly higher percentage of snow ablation on CSG compared to DBG is probably due to the reason that it gets around 53% of its annual precipitation in winter months that melt out in the summer-monsoon months while DBG receives 74% of its annual precipitation in the summer-monsoon when T_a is the highest which might result in rainfall on DBG even up to 5,100 m a.s.l. (Pratap et al., 2015) (Section Meteorological Conditions and Seasonal Characteristics). Under similar mass wastage conditions (Section Glacier-Wide Annual and Seasonal Mass Balances), the percent contribution of melt from debris-covered ice on DBG was three times of CSG due to three-folds of debris-covered ice on DBG (∼13%) compared to CSG (∼4%) (Vincent et al., 2013; Pratap et al., 2015).

DISCUSSION

SEB in Ablation and Accumulation Zones

Most of the SEB studies in the HK have been performed at point-scale in the ablation zones (Azam et al., 2018; Litt et al., 2019). However, a few glacier-wide studies suggested that SEB is quite different in the ablation and accumulation zones of glaciers (Sun et al., 2014; Patel et al., 2021). To investigate the SEB in the ablation and accumulation zones of DBG and CSG, we estimated the mean annual ablation-wide and accumulation-wide SEBs separately, dividing the ablation and accumulation zones using the mean ELA from the literature (**Table 1**).

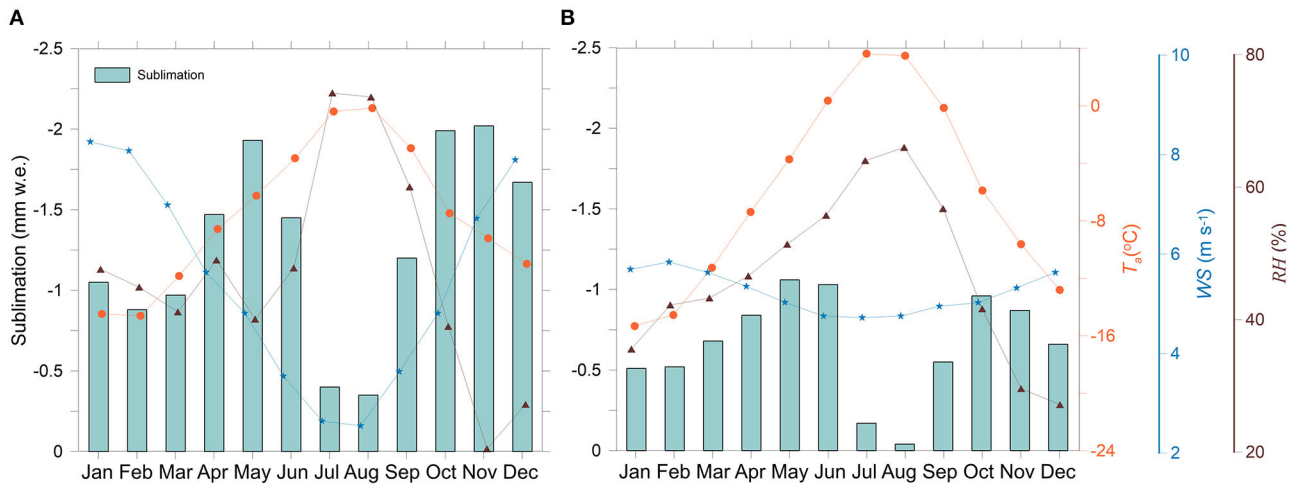

FIGURE 9 | Monthly mean glacier-wide T_a (orange dots), *RH* (brown triangles), *WS* (blue stars), sublimation (blue-green bars) on **(A)** DBG and **(B)** CSG.

Mean monthly *SWN* budgets were similar over the ablation zones of both the glaciers: strong mean monthly cycles had the highest *SWN* in August during the summer monsoon and the lowest *SWN* in the winter, while relatively moderate values in the accumulation zone throughout the year except the winter when *SWN* were the lowest on both the glaciers (**Supplementary Table S6**; **Figure 10**). In winter, both the glaciers were completely covered by snow which resulted in higher surface albedo and similar ablation- and accumulation-wide *SWN* budgets (**Supplementary Table S6**). Negative *LWN* budgets showed higher loss of energy in the ablation zone compared to the accumulation zone throughout the year with most negative values in winter on both the glaciers (**Supplementary Table S6**; **Figure 10**), except slightly positive values in July–August on DBG most probably due to the highest *LWI* of heavy monsoonal cloud cover (**Supplementary Table S4**). Mean monthly *H* were positive as T_a was higher than T_s in the ablation zones of both the glaciers, while negative in the accumulation zones during the summer monsoon and pre-monsoon (**Supplementary Table S6**; **Figure 10**) as T_s becomes higher than T_a on both the glaciers (**Supplementary Table S4**). The *LE* was consistently negative in the accumulation zones of both the glaciers suggesting continuous mass loss through sublimation from higher altitudes; however it was slightly positive in the ablation zones over July–August on both the glaciers indicating re-sublimation during the core summer-monsoon (**Figure 10**). The resublimation was 3.50 and 2.04% on DBG and CSG respectively, compared to sublimation in the ablation zone. The value, *Q* remained negative throughout the year except for the summer monsoon in the ablation zones and July–August in the accumulation zones due to higher *SWN* on both the glaciers. Similar results have been discussed in other SEB studies on the Himalayan glaciers (Azam et al., 2014b; Litt et al., 2019; Patel et al., 2021).

Major Drivers for Glacier Mass Balances

Due to the scarcity of mass balance and meteorological data in the HK, the climatic drivers controlling the mass balances have been poorly discussed (Azam et al., 2014a, 2018; Shea et al., 2015a). To comprehend the major drivers controlling the glacier-wide seasonal and annual mass balances, the correlation coefficients (*r*) were developed amid annual and seasonal mass balances, bias-corrected mean annual ERA5 data, and surface energy fluxes over 1979–2020 on both the glaciers (**Figure 11**).

The value of B_a on DBG showed strong positive correlations (r = ∼0.40–0.70) with *P* and surface albedo while moderately negative correlations (r = ∼0.40–0.60) with *SWN*, R_n, and *Q* (**Figure 11**). Similarly, CSG also showed good correlations with *P* and surface albedo; however, the negative correlations with *SWN*, R_n and *Q* were stronger (r = ∼0.80) (**Figure 11**). Due to their undersized role in total SEB (Section Seasonal and Annual Glacier-Wide Surface Energy Balance), *H*, *LE*, and *LWN* showed insignificant correlations with annual as well as seasonal mass balances on both the glaciers (**Figure 11**).

The value of B_a and summer mass balances on CSG showed moderate correlations with *SWI* while these correlations on DBG were insignificant (**Figure 11**). This is probably due to heavy monsoonal clouds that reduce the amount of *SWI* on DBG, resulting in low mean annual values (**Supplementary Table S4**). Winter mass balances on DBG showed weak positive correlation (r = 0.27) with *P* while a stronger positive correlation (r = 0.63) was observed on CSG (**Figure 11**). This is expected as DBG and CSG are summer and winter accumulation-type glaciers, respectively (Section Meteorological Conditions and Seasonal Characteristics). Further, summer mass balances on both the glaciers showed moderately positive but almost similar correlations (r = ∼0.60) with *P* (**Figure 11**). Despite the fact that CSG receives its major annual precipitation during winter, almost similar correlation between summer mass balances and

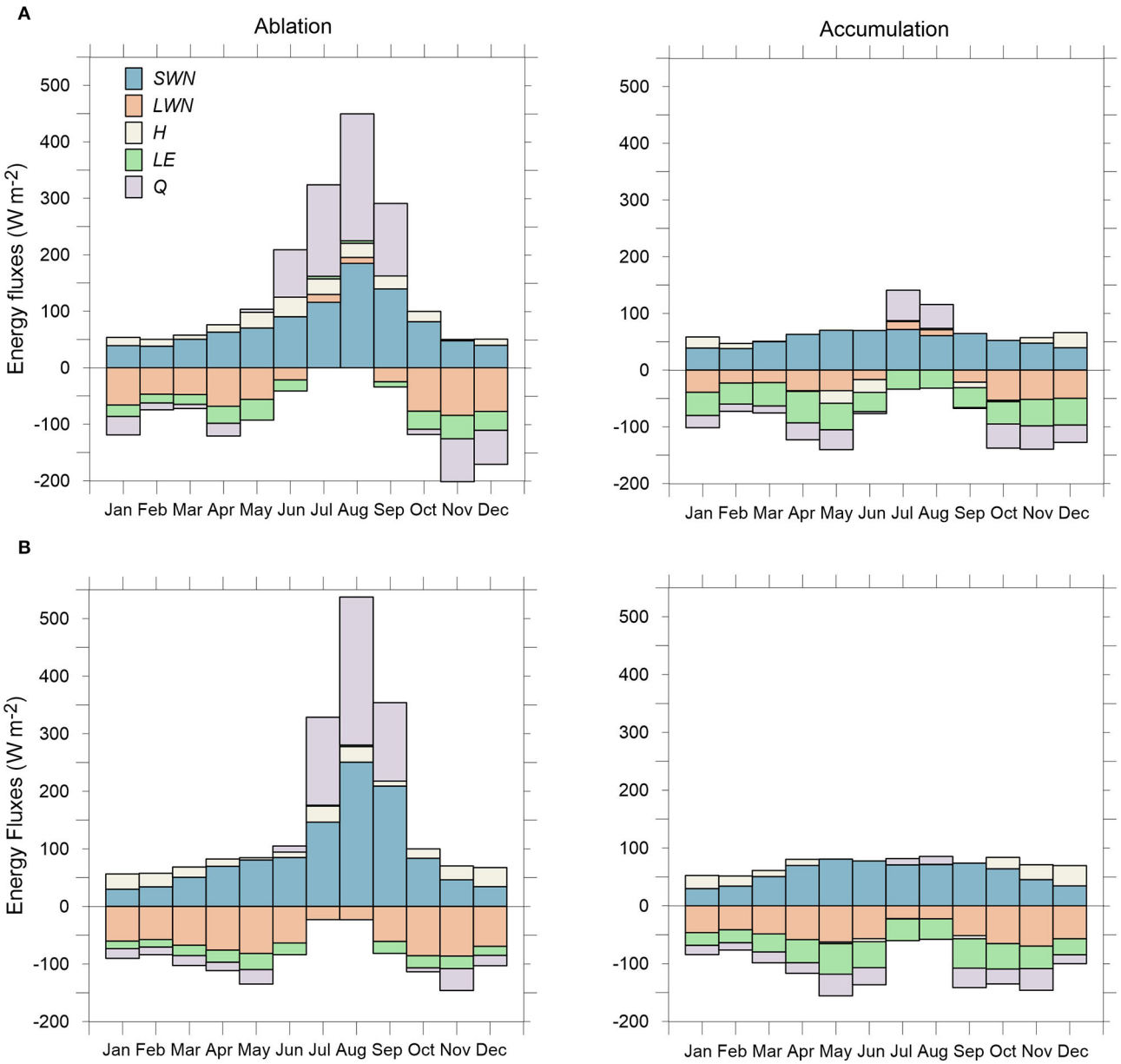

FIGURE 10 | SEB in ablation and accumulation zones of **(A)** DBG and **(B)** CSG.

P occurs most probably due to sporadic summer-monsoonal snowfall events on CSG (Azam et al., 2019). A previous study on CSG investigated the critical role of summer-monsoon snowfalls in detail and concluded that these snowfalls often cover the whole or part of the ablation zone during peak melting months and abruptly reduce the *SWI* absorption and control the summer mass balances which further control the B_a (Azam et al., 2014b). The value of T_a showed weak and moderate negative correlations with B_a ($r = -0.30$) and summer ($r = -0.52$) mass balances, respectively on DBG, while showed moderate negative correlations with B_a ($r = -0.44$) and summer ($r = -0.40$) mass balances (**Figure 11**). The value of T_a was poorly correlated with winter mass balances on both the glaciers (**Figure 11**). However, as expected, T_a showed very strong correlations with T_s and *LWO* on both the glaciers (**Figure 11**).

The value of B_a on DBG and CSG showed moderately strong correlations with winter mass balances ($r = 0.58$ and $r = 0.67$, respectively) while showing very strong correlations with summer mass balances ($r = 0.80$, $r = 0.97$, respectively) (**Figure 11**). Higher dependency of B_a on summer mass balances suggests that both the glaciers have high vulnerability to regional warming; hence, expected to lose more mass in the continuation of warming (Banerjee and Azam, 2016; Kraaijenbrink et al., 2017; Krishnan et al., 2019; Mahto and Mishra, 2019).

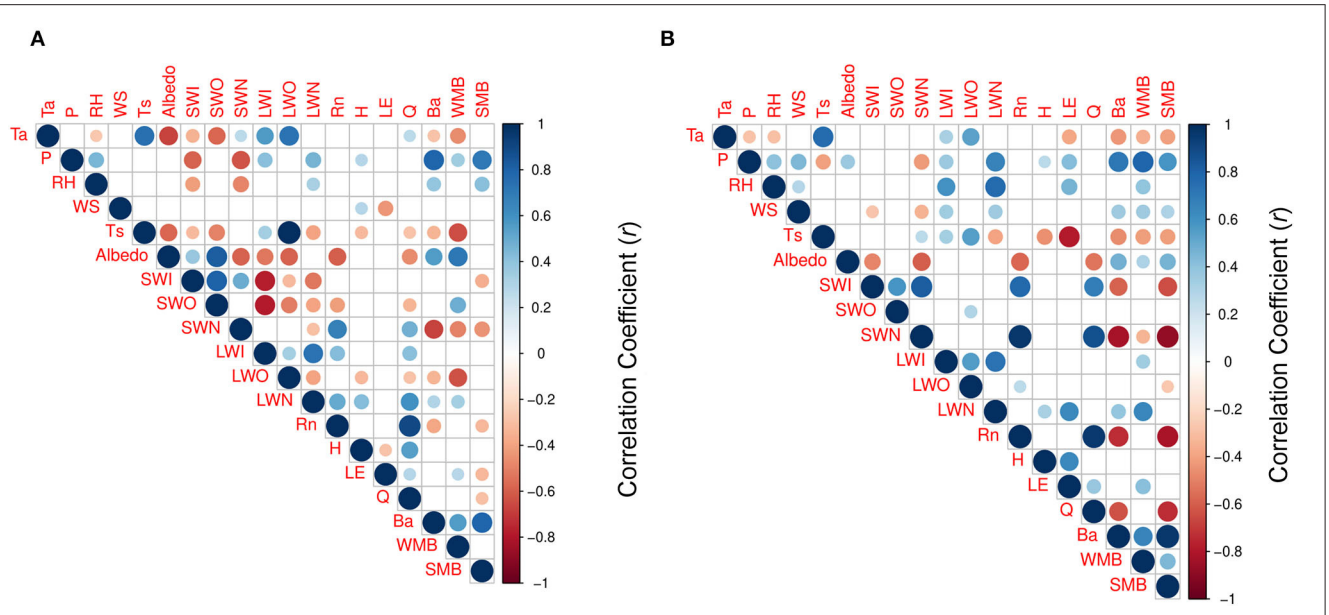

FIGURE 11 | (A,B) A graphical representation of correlations with 1% (0.01) *p* significance values among the inter-annual variability of mass balance, energy fluxes and its meteorological drivers during 1979–2020 for DBG and CSG, respectively (red color shows negative while blue color shows positive correlation values). WMB and SMB are winter and summer mass balances.

Annual Glacier-Wide Mass Balance Sensitivity

Mass balance sensitivities were computed to understand the response of the glaciers to the changes in different model input parameters. These sensitivities were computed, one-by-one, by re-running the model with a unique set of each model parameter where h_H was the highest and h_L was the lowest value of parameter h, holding all the other parameters constant. Following Ragettli et al. (2013), the h_H and h_L were estimated by varying each parameter h by ±10% from its calibrated value except for T_m, T_p, T_a which were varied by 0.1, 0.1, and 1.0°C, respectively (**Table 2**). The mass balance sensitivities were estimated for the period 1979–2020 following (Oerlemans et al., 1998):

$$\frac{dB_a}{dh} = \frac{B_a\ (h_H) - B_a\ (h_L)}{2} \tag{17}$$

Where, B_a is the glacier-wide mass balance averaged over the period 1979–2020.

The estimated B_a sensitivities on DBG and CSG are given in **Table 2**. The B_a was the most sensitive to α_s, with the sensitivities of 0.29 and 0.37 m w.e. a^{-1} on DBG and CSG, respectively (**Table 2**). Previous studies on other glaciers in the Alps and Himalaya also showed the maximum sensitivity of $B_a$to α_s (Klok and Oerlemans, 2004; Johnson and Rupper, 2020; Stigter et al., 2021). The modeled B_a showed moderate sensitivities to T_{LR} (DBG = 0.10 m w.e. a^{-1}; CSG = 0.12 m w.e. a^{-1}). Sensitivities were quite low to T_p, T_M, α_d, α_i and P_G for both the glaciers (**Table 2**).

The sensitivity of the modeled mean B_a to 1°C change in T_a was higher on DBG (−0.50 m w.e. a^{-1}) than CSG (−0.30 m w.e. a^{-1}) whereas the sensitivities to 10% change in P were roughly the same (DBG = 0.23 m w.e. a^{-1}, CSG = 0.13 m w.e. a^{-1}) (**Table 2**). Higher sensitivity to T_a on DBG is probably due to different precipitation regimes on both the glaciers. DBG receives its maximum of annual precipitation in the summer monsoon when T_a is the highest; hence, DBG had more sensitivity to T_a compared to CSG that receives its major precipitation in winters (Fujita, 2008; Azam et al., 2014a). Using a T-index model, a previous study on CSG computed higher sensitivity (−0.52 m w.e. a^{-1}) of mass balance to 1°C change in T_a and roughly similar sensitivity (0.16 m w.e. a^{-1}) to 10% change in P (Azam et al., 2014a). Another study on Zhadang Glacier in Tibet showed similar results using an energy balance model with the sensitivity of −0.47 m w.e. a^{-1} to 1°C change in T_a and sensitivity of 0.14 m w.e. a^{-1} to 10% change in P (Mölg et al., 2012). Our sensitivity results are quite comparable with these studies in the mountain glaciers.

Comparison of Sublimation Rates With HK Glaciers

In this section, we discuss the sublimation rates from different studies on HK glaciers. However, irrespective of our glacier-wide and round-the-year study, often the studies were (i) available at point-scale, (ii) from different months of the year, (iii) having different locations of automatic weather stations (on/off glacier), and (iv) installed on different surfaces (snow and ice) that hinders a direct comparison. In the present study, the mean glacier-wide sublimation was computed as −1.28 and −0.66 mm w.e. d^{-1} over 1979–2020 on DBG and CSG, respectively. Previously, using *in-situ* AWS data from the middle of the ablation zone (4,670 m a.s.l.) on CSG, a point-scale SEB study computed a mean sublimation of −0.63 mm w.e. d^{-1} over 2012–2013 (Azam et al., 2014a). Another recent point-scale SEB study on seasonal snow

surface on a lateral moraine of CSG only (4,863 m a.s.l.) suggested that sublimation was -1.1 mm d^{-1} during winters over 2009–2020 (Mandal et al., 2022). The mean glacier-wide sublimation was reported as -1.08 and -0.70 mm w.e. d^{-1} on Zhadang Glacier (south-central Tibetan Plateau) and on Puruogangri ice (north-central Tibetan Plateau) between 2001 and 2011 (Huintjes et al., 2015a,b). In the central Himalaya, the sublimation rate was reported for short-term snow-cover at the Pindari Glacier AWS site (off-glacier; 3750 m a.s.l.) to be -0.3 mm d^{-1} during winters (Singh et al., 2020). In the Nepal Himalaya, on Yala Glacier (5350 m a.s.l.) around -1.00 mm d^{-1} mass was lost through sublimation during winters (Stigter et al., 2018). In line, another study showed significant sublimation rate of -7.1 and -1.9 mm d^{-1} on Mera Glacier and -2.4 and -1.8 mm d^{-1} on Yala Glacier during the post- and pre-monsoon season, respectively (Litt et al., 2019).

Mass Balance Comparison With Other Studies

The *in-situ* glaciological method showed a mass wastage of -0.32 m w.e. a^{-1} on DBG over 1992–1995, 1997–2000, and 2007–2013 (Dobhal et al., 2021), while our model showed slightly lesser mass wastage of -0.27 ± 0.31 m w.e. a^{-1} over the same years (**Figure 12A**). On CSG, the glaciological method showed a mass wastage of -0.43 ± 0.40 m w.e. a^{-1} over 2002–2019 (Mandal et al., 2020), while our model showed similar mass wastage of -0.42 ± 0.42 m w.e. a^{-1} (**Figure 12B**).

Geodetic mass balances are also available on both the glaciers and are used here to validate the modeled mass-balance series. A recent study using high-resolution Cartosat-1 DEM and SRTM DEM estimated a mass wastage of -0.23 ± 0.10 m w.e. a^{-1} on DBG over 1999–2014 (Garg et al., 2021). Over the same period, our model showed slightly higher mass wastage with a mean mass balance of -0.35 ± 0.41 m w.e. a^{-1} on DBG. On CSG, our model showed higher mass wastage of -0.39 ± 0.43 m w.e. a^{-1} against a mass wastage of -0.27 ± 0.13 m w.e. a^{-1} over 2005–2014 derived using ASTER DEMs (Brun et al., 2017). Another geodetic study provided a mean mass wastage of -0.46 ± 0.34 m w.e. a^{-1} over 2000–2012 (Vijay and Braun, 2016), while our model computed a mean mass wastage of -0.67 ± 0.54 m w.e. a^{-1} over the same period. Another geodetic study combining SRTM and SPOT5 DEMs provided a mean mass wastage of -1.12 m w.e. a^{-1} using density assumption 1 and -1.02 m w.e. a^{-1} using density assumption 2 which is in close agreement with our model value (-1.01 m w.e. a^{-1}) over 1999–2004 (Berthier et al., 2007) (**Figures 12A,B**).

Our modeled mean mass balance of -0.27 ± 0.39 m w.e. a^{-1} on DBG and -0.31 ± 0.38 m w.e. a^{-1} on CSG were in better agreement with the modeled mean mass balance of -0.25 ± 0.37 m w.e. a^{-1} and -0.26 ± 0.29 m w.e. a^{-1} from a simplified T-index model over 1979–2020 (Srivastava et al., 2021). The present study, showing a moderate mean mass balance on both the glaciers over 1979–2020, is in close agreement with most of the previous studies and nicely captures the inter-annual variability with other modeled MBs (**Figures 12A,B**).

CONCLUSION

Due to harsh climatic conditions, long-term *in-situ* glacio-meteorological observations are sparse in the HK region, which impedes an in-depth understanding of the glacier–climate relationship. A mass- and energy-balance model is used to get around this constraint, using the long-term ERA5 reanalysis data since 1979, for two climatically diverse glaciers of DBG and CSG where a fairly good amount of *in-situ* glacio-meteorological data are available from previous studies. The *in-situ* measurements are used to calibrate/validate the model for DBG and CSG. The model is further used to study the altitudinal patterns of mass balance and surface energy fluxes over both the glaciers.

Both the glaciers experience a warm and moist weather condition with low wind velocity during the summer monsoon (June–September) and a cold, dry windy condition during winter (December to March). Intermediate weather conditions persist during pre-monsoon (April to May) and post-monsoon (October-November). DBG receives the majority of precipitation (∼74%) in the summer monsoon whereas CSG receives maximum precipitation (∼53%) in winter.

DBG and CSG are losing mass at a moderate rate with the mean B_a of -0.27 ± 0.32 m w.e. a^{-1} and -0.31 ± 0.38 m w.e. a^{-1}, respectively, over 1979–2020. Though the mean mass wastage on both the glaciers is similar, the annual mass turnover on CSG is higher than that on DBG. The mean summer and winter mass balances are computed to be -0.60 ± 0.30 and 0.32 ± 0.02 m w.e. a^{-1} on DBG and -0.79 ± 0.36 and 0.48 ± 0.02 m w.e. a^{-1} on CSG, respectively.

Glacier-wide net shortwave radiation has the dominant control over energy balance followed by longwave net radiation, latent heat flux, and sensible heat flux on both the glaciers. On the annual scale, both DBG and CSG showed a positive glacier-wide net energy of 10 W m^{-2} indicating a mass wastage over 1979–2020. Latent heat flux is always negative suggesting glacier-wide sublimation throughout the year except for peak summer monsoon when it is slightly positive over ablation zone indicating re-sublimation on both the glaciers. The losses through sublimation are around 22 and 20% of total ablation on DBG and CSG, respectively, with a strong spatial and temporal variability.

The value of B_a on DBG and CSG showed moderately strong correlations with winter mass balances, while showing very strong correlations with summer-mass balances, suggesting summer as the main mass balance driver season. The sensitivity of modeled mean B_a to 1°C change in T_a is higher on DBG (-0.50 m w.e. a^{-1}) than the CSG (-0.30 m w.e. a^{-1}) whereas the sensitivities to 10% change in P are nearly the same (DBG = 0.23 m w.e. a^{-1}, CSG = 0.13 m w.e. a^{-1}) over 1979–2020. Mass- and energy-balance model is the most sensitive to snow albedo followed by temperature lapse rates and least sensitivity to the rest of the model parameters on both the glaciers.

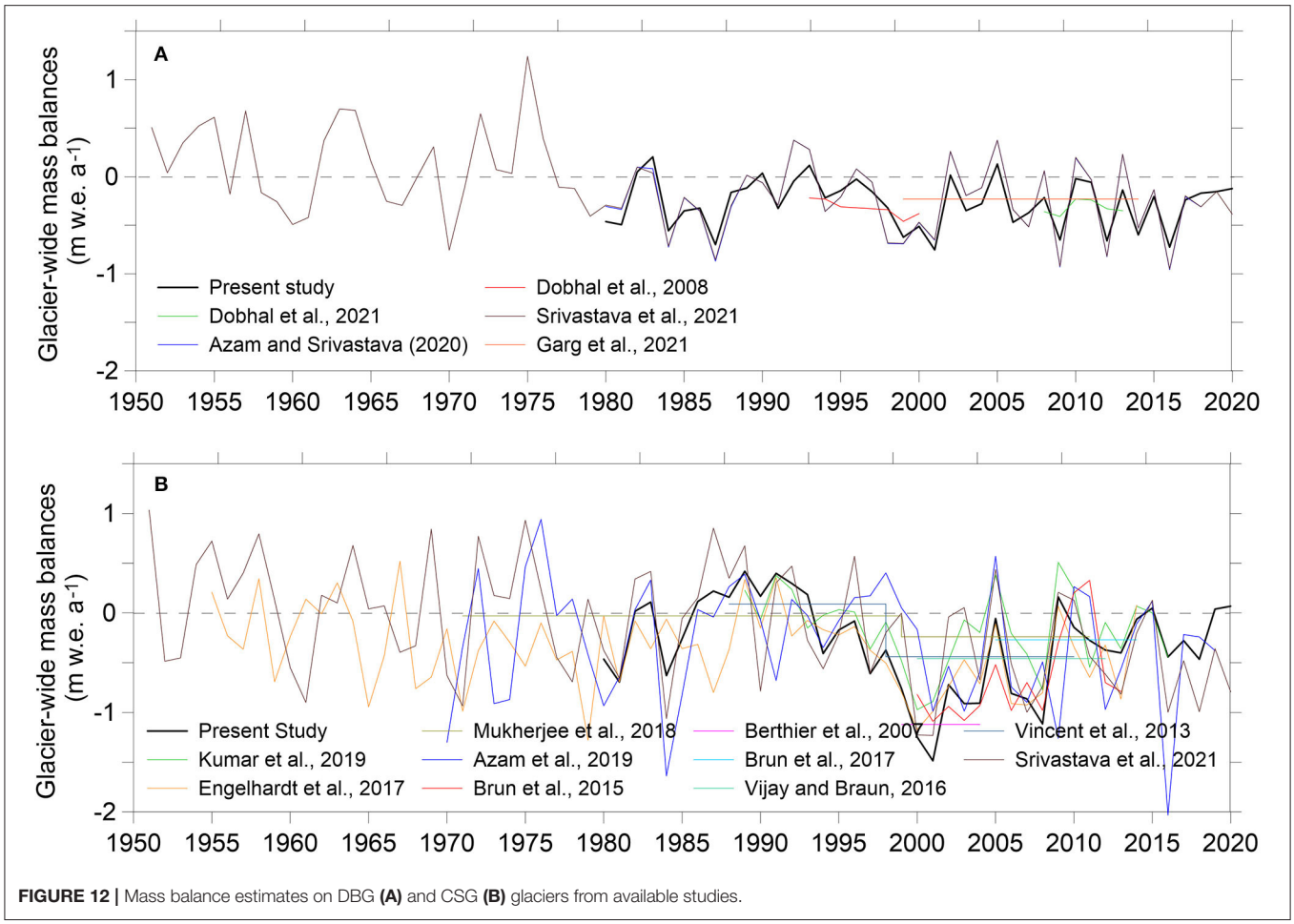

FIGURE 12 | Mass balance estimates on DBG **(A)** and CSG **(B)** glaciers from available studies.

The modeled B_a on both the glaciers show a good agreement with the available mass balances from geodetic, model, and *in-situ* measurements. This study provides insights into the regional variations in mass-wastage governing SEB fluxes at glacier-wide scale, which is helpful for understanding the glacier–climate interactions in the Himalaya and stresses an inclusion of a sublimation scheme in T-index models. A possible, rapid advancement could be to assimilate the simplified scheme of sublimation, such as the empirical equation in T-index models of Kuchment and Gelfan (1996). However, such equations need to be tested for their transferability from one region to other.

DATA AVAILABILITY STATEMENT

The original contributions presented in the study are included in the article/**Supplementary Material**, further inquiries can be directed to the corresponding author/s.

AUTHOR CONTRIBUTIONS

MFA designed the study. SS developed the model and figures. SS and MFA did the analysis and wrote the paper. All authors contributed to the article and approved the submitted version.

FUNDING

SS acknowledges the research fellowship from the Space Application Centre (ISRO) through the Cryospheric Science and Application Program. MFA acknowledges the research grant from INSPIRE Scheme (IFA-14-EAS-22), from the Department of Science and Technology (DST, India), and the Core Research Grant (CRG/2020/004877) from Science and Engineering Research Board (SERB), DST, India.

ACKNOWLEDGMENTS

The authors acknowledge the European Centre for Medium-Range Weather Forecasts (ECMWF) for keeping the data publicly accessible. The authors also thank the scientists who have collected the *in-situ* data on both the glaciers. A special thanks to Dr. Rajdeep for the stylistic improvement of the manuscript.

SUPPLEMENTARY MATERIAL

The Supplementary Material for this article can be found online at: https://www.frontiersin.org/articles/10.3389/frwa.2022.874240/full#supplementary-material

REFERENCES

Acharya, A., and Kayastha, R. B. (2019). Mass and energy balance estimation of Yala glacier (2011–2017), Langtang valley, Nepal. *Water* 11, 6. doi: 10.3390/w11010006

Anslow, F. S., Hostetler, S., Bidlake, W. R., and Clark, P. U. (2008). Distributed energy balance modeling of South Cascade Glacier, Washington and assessment of model uncertainty. *J. Geophys. Res. Earth Surf.* 113, F2. doi: 10.1029/2007JF000850

Azam, M. F. (2021). Need of integrated monitoring on reference glacier catchments for future water security in Himalaya. *Water Secur*. 14, 100098. doi: 10.1016/j.wasec.2021.100098

Azam, M. F., Kargel, J. S., Shea, J. M., Nepal, S., Haritashya, U. K., Srivastava, S., et al. (2021). Glaciohydrology of the himalaya-karakoram. *Science* 373, eabf3668. doi: 10.1126/science.abf3668

Azam, M. F., Ramanathan, A. L., Wagnon, P., Vincent, C., Linda, A., Berthier, E., et al. (2016). Meteorological conditions, seasonal and annual mass balances of Chhota Shigri Glacier, western Himalaya, India. *Ann. Glaciol.* 57, 328–338. doi: 10.3189/2016AoG71A570

Azam, M. F., and Srivastava, S. (2020). Mass balance and runoff modelling of partially debris-covered Dokriani Glacier in monsoon-dominated Himalaya using ERA5 data since 1979. *J. Hydrol.* 590, 125432. doi: 10.1016/j.jhydrol.2020.125432

Azam, M. F., Wagnon, P., Berthier, E., Vincent, C., Fujita, K., and Kargel, J. S. (2018). Review of the status and mass changes of Himalayan-Karakoram glaciers. *J. Glaciol.* 64, 61–74. doi: 10.1017/jog.2017.86

Azam, M. F., Wagnon, P., Vincent, C., Ramanathan, A., Linda, A., and Singh, V. B. (2014a). Reconstruction of the annual mass balance of Chhota Shigri glacier, Western Himalaya, India, since 1969. *Ann. Glaciol.* 55, 6980. doi: 10.3189/2014AoG66A104

Azam, M. F., Wagnon, P., Vincent, C., Ramanathan, A. L., Favier, V., Mandal, A., et al. (2014b). Processes governing the mass balance of Chhota Shigri Glacier (western Himalaya, India) assessed by point-scale surface energy balance measurements. *Cryosphere* 8, 2195–2217. doi: 10.5194/tc-8-2195-2014

Azam, M. F., Wagnon, P., Vincent, C., Ramanathan, A. L., Kumar, N., Srivastava, S., et al. (2019). Snow and ice melt contributions in a highly glacierized catchment of Chhota Shigri Glacier (India) over the last five decades. *J. Hydrol.* 574, 760–773. doi: 10.1016/j.jhydrol.2019.04.075

Banerjee, A. (2017). Brief communication: Thinning of debris-covered and debris-free glacier in a warming climate. *Cryosphere* 11, 133–138. doi: 10.5194/tc-11-133-2017

Banerjee, A., and Azam, M. F. (2016). Temperature reconstruction from glacier length fluctuations in the Himalaya. *Ann. Glaciol.* 57, 189–198. doi: 10.3189/2016AoG71A047

Berthier, E., Arnaud, Y., Kumar, R., Ahmad, S., Wagnon, P., and Chevallier, P. (2007). Remote Sens. estimates of glacier mass balances in the Himachal Pradesh (Western Himalaya, India). *Remote Sens. Environ.* 108, 327–338. doi: 10.1016/j.rse.2006.11.017

Berthier, E., and Brun, F. (2019). Karakoram geodetic glacier mass balances between 2008 and 2016: persistence of the anomaly and influence of a large rock avalanche on Siachen Glacier. *J. Glaciol.* 65, 494–507. doi: 10.1017/jog.2019.32

Bolch, T., Pieczonka, T., Mukherjee, K., and Shea, J. (2017). Brief communication: glaciers in the Hunza catchment (Karakoram) have been nearly in balance since the 1970s. *Cryosphere* 11, 531–539. doi: 10.5194/tc-11-531-2017

Bolch, T., Shea, J. M., Liu, S., Azam, F. M., Gao, Y., Gruber, S., et al. (2019). "Status and change of Cryosphere in the extended Hindu Kush Himalaya region," in *The Hindu Kush Himalaya Assessment* (Cham: Springer), 209–255

Brock, B. W., and Arnold, N. S. (2000). A spreadsheet-based (Microsoft Excel) point surface energy balance model for glacier and snow melt studies. *Earth Surf. Process. Landf.* 25, 649–658. doi: 10.1002/1096-9837(200006)25:6<649::AID-ESP97>3.0.CO;2-U

Brun, F., Berthier, E., Wagnon, P., Kääb, A., and Treichler, D. (2017). A spatially resolved estimate of High Mountain Asia glacier mass balances from 2000 to 2016. *Nat. Geosci.* 10, 668–673. doi: 10.1038/ngeo2999

Brun, F., Dumont, M., Wagnon, P., Berthier, E., Azam, M. F., Shea, J. M., et al. (2015). Seasonal changes in surface albedo of Himalayan glaciers from MODIS data and links with the annual mass balance. *Cryosphere* 9, 341–355. doi: 10.5194/tc-9-341-2015

Copernicus Climate Change Service (C3S) (2017). ERA5. Available online at: https://cds.climate.copernicus.eu/cdsapp#!/home (accessed April 6, 2022).

Cuffey, K. M., and Paterson, W. S. B. (2010). *The Physics of Glaciers*. Academic Press.

de Kok, R. J., Tuinenburg, O. A., Bonekamp, P. N., and Immerzeel, W. W. (2018). Irrigation as a potential driver for anomalous glacier behavior in High Mountain Asia. *Geophys. Res. Lett.* 45, 2047–2054. doi: 10.1002/2017GL076158

Denby, B., and Greuell, W. (2000). The use of bulk and profile methods for determining surface heat fluxes in the presence of glacier winds. *J. Glaciol.* 46, 445–452. doi: 10.3189/172756500781833124

Dimri, A. P., Yasunari, T., Kotlia, B. S., Mohanty, U. C., and Sikka, D. R. (2016). Indian winter monsoon: present and past. *Earth-Sci. Rev.* 163, 297–322. doi: 10.1016/j.earscirev.2016.10.008

Dobhal, D. P., Gergan, J. T., and Thayyen, R. J. (2008). Mass balance studies of the Dokriani Glacier from to, Garhwal Himalaya, India. *Bull. Glaciol. Res.* 25, 9–17.

Dobhal, D. P., Pratap, B., Bhambri, R., and Mehta, M. (2021). Mass balance and morphological changes of Dokriani Glacier (1992–2013), Garhwal Himalaya, India. *Quat. Sci. Adv.* 4, 100033. doi: 10.1016/j.qsa.2021.100033

Engelhardt, M., Ramanathan, A. L., Eidhammer, T., Kumar, P., Landgren, O., Mandal, A., et al. (2017). Modelling 60 years of glacier mass balance and runoff for Chhota Shigri Glacier, Western Himalaya, Northern India. *J. Glaciol.* 63, 618–628. doi: 10.1017/jog.2017.29

Farinotti, D., Immerzeel, W. W., De Kok, R. J., Quincey, D. J., and Dehecq, A. (2020). Manifestations and mechanisms of the Karakoram glacier. *Anomaly Nat. Geosci*. 13, 8–16. doi: 10.1038/s41561-019-0513-5

Favier, V., Wagnon, P., Chazarin, J. P., Maisincho, L., and Coudrain, A. (2004). One-year measurements of surface heat budget on the ablation zone of Antizana Glacier 15, Ecuadorian Andes. *J. Geophys. Res. Atmos.* 109, D18. doi: 10.1029/2003JD004359

Fujita, K. (2008). Effect of precipitation seasonality on climatic sensitivity of glacier mass balance. *Earth Planet. Sci. Lett.* 276, 14–19. doi: 10.1016/j.epsl.2008.08.028

Fujita, K., and Ageta, Y. (2000). Effect of summer accumulation on glacier mass balance on the Tibetan Plateau revealed by mass-balance model. *J. Glaciol.* 46, 244–252. doi: 10.3189/172756500781832945

Fujita, K., and Sakai, A. (2014). Modelling runoff from a Himalayan debris-covered glacier. *Hydrol. Earth Syst. Sci.* 18, 2679–2694. doi: 10.5194/hess-18-2679-2014

Fujita, K., Takeuchi, N., Nikitin, S. A., Surazakov, A. B., Okamoto, S., Aizen, V. B., et al. (2011). Favorable climatic regime for maintaining the present-day geometry of the Gregoriev Glacier, Inner Tien Shan. *Cryosphere* 5, 539–549. doi: 10.5194/tc-5-539-2011

Gadgil, S., Vinayachandran, P. N., and Francis, P. A. (2003). Droughts of the Indian summer monsoon: role of clouds over the Indian Ocean. *Curr. Sci.* 85, 1713–9. Available online at: https://www.jstor.org/stable/24109976

Gardelle, J., Berthier, E., and Arnaud, Y. (2012). Slight mass gain of Karakoram glaciers in the early twenty-first century. *Nat. Geosci.* 5, 322–325. doi: 10.1038/ngeo1450

Garg, P. K., Yadav, J. S., Rai, S. K., and Shukla, A. (2021). Mass balance and morphological evolution of the Dokriani Glacier, central Himalaya, India during 1999–2014. *Geosci. Front.* 13, 101290. doi: 10.1016/j.gsf.2021.101290

Haq, M. A., Azam, M. F., and Vincent, C. (2021). Efficiency of artificial neural networks for glacier ice-thickness estimation: a case study in western Himalaya, India. *J. Glaciol.* 264, 1–14. doi: 10.1017/jog.2021.19

Hay, J. E., and Fitzharris, B. B. (1988). A comparison of the energy-balance and bulk-aerodynamic approaches for estimating glacier melt. *J. Glaciol.* 34, 145–153. doi: 10.1017/S0022143000032172

Hewitt, K. (2005). The Karakoram anomaly? Glacier expansion and the 'elevation effect,'Karakoram Himalaya. *Mt. Res. Dev.* 25, 332–340. doi: 10.1659/0276-4741(2005)0250332:TKAGEA2.0.CO;2

Hock, R. (2003). Temperature index melt modelling in mountain areas. *J. Hydrol.* 282, 104–115. doi: 10.1016/S0022-1694(03)00257-9

Hock, R., Rasul, G., Adler, C., Cáceres, B., Gruber, S., Hirabayashi, Y., et al. (2019). "High mountain areas," in *IPCC Special Report on Ocean and the Cryosphere in a Changing Climate* (Geneva: IPCC).

Huintjes, E., Neckel, N., Hochschild, V., and Schneider, C. (2015a). Surface energy and mass balance at Purogangri ice cap, central Tibetan Plateau, 2001–2011. *J. Glaciol.* 61, 1048–1060. doi: 10.3189/2015JoG15J056

Huintjes, E., Sauter, T., Schröter, B., Maussion, F., Yang, W., Kropáček, J., et al. (2015b). Evaluation of a coupled snow and energy balance model for Zhadang glacier, Tibetan Plateau, using glaciological measurements and time-lapse photography. *Arct. Antarct. Alp. Res*. 47, 573–590. doi: 10.1657/AAAR0014-073

Huss, M., Farinotti, D., Bauder, A., and Funk, M. (2008). Modelling runoff from highly glacierized alpine drainage basins in a changing climate. *Hydrol. Process.* 22, 3888–3902. doi: 10.1002/hyp.7055

Immerzeel, W. W., Lutz, A. F., Andrade, M., Bahl, A., Biemans, H., Bolch, T., et al. (2020). Importance and vulnerability of the world's water towers. *Nature* 577, 364–369. doi: 10.1038/s41586-019-1822-y

Immerzeel, W. W., Wanders, N., Lutz, A. F., Shea, J. M., and Bierkens, M. F. P. (2015). Reconciling high-altitude precipitation in the upper Indus basin with glacier mass balances and runoff. *Hydrol. Earth Syst. Sci*. 19, 4673–4687. doi: 10.5194/hess-19-4673-2015

Jennings, K. S., Winchell, T. S., Livneh, B., and Molotch, N. P. (2018). Spatial variation of the rain–snow temperature threshold across the Northern Hemisphere. *Nat. Commun*. 9, 1–9. doi: 10.1038/s41467-018-03629-7

Johnson, E., and Rupper, S. (2020). An examination of physical processes that trigger the albedo-feedback on glacier surfaces and implications for regional glacier mass balance across High Mountain Asia. *Front. Earth Sci*. 8, 129. doi: 10.3389/feart.2020.00129

Kääb, A., Treichler, D., Nuth, C., and Berthier, E. (2015). Brief Communication: Contending estimates of 2003–2008 glacier mass balance over the Pamir–Karakoram–Himalaya. *Cryosphere* 9, 557–564. doi: 10.5194/tc-9-557-2015

Kayastha, R. B., Ohata, T., and Ageta, Y. (1999). Application of a mass-balance model to a Himalayan glacier. J. *Glaciol*. 45, 559–567. doi: 10.1017/S002214300000143X

Klok, E. J., and Oerlemans, J. (2004). Modelled climate sensitivity of the mass balance of Morteratschgletscher and its dependence on albedo parameterization. *Int. J. Climatol*. 24, 231–245. doi: 10.1002/joc.994

Konz, M., and Seibert, J. (2010). On the value of glacier mass balances for hydrological model calibration. *J. Hydrol*. 385, 238–246. doi: 10.1016/j.jhydrol.2010.02.025

Kraaijenbrink, P. D., Bierkens, M. F. P., Lutz, A. F., and Immerzeel, W. W. (2017). Impact of a global temperature rise of 1.5 degrees Celsius on Asia's glaciers. *Nature* 549, 257–260. doi: 10.1038/nature23878

Krishnan, R., Shrestha, A. B., Ren, G., Rajbhandari, R., Saeed, S., Sanjay, J., et al. (2019). "Unravelling climate change in the Hindu Kush Himalaya: rapid warming in the mountains and increasing extremes," in *The Hindu Kush Himalaya Assessment* (Cham: Springer), 57–97.

Kuchment, L. S., and Gelfan, A. N. (1996). The determination of the snowmelt rate and the meltwater outflow from a snowpack for modelling river runoff generation. *J. Hydrol*. 179, 23–36. doi: 10.1016/0022-1694(95)02878-1

Kumar, A., Negi, H. S., and Kumar, K. (2020). Long-term mass balance modelling (1986–2018) and climate sensitivity of Siachen Glacier, East Karakoram. *Environ. Monit. Assess.* 192, 1–16. doi: 10.1007/s10661-020-08323-0

Kumar, A., Negi, H. S., and Kumar, K. (2021). Long-term (∼ 40 years) mass balance appraisal and response of the Patsio glacier, in the Great Himalayan region towards climate change. J. *Earth Syst. Sci*. 130, 1–12. doi: 10.1007/s12040-021-01555-9

Kumar, P., Saharwardi, M. S., Banerjee, A., Azam, M. F., Dubey, A. K., and Murtugudde, R. (2019). Snowfall variability dictates glacier mass balance variability in Himalaya-Karakoram. *Sci. Rep*. 9, 1–9. doi: 10.1038/s41598-019-54553-9

Kumar, R., Singh, S., Kumar, R., Singh, A., Bhardwaj, A., Sam, L., et al. (2016). Development of a glacio-hydrological model for discharge and mass balance reconstruction. *Water Resour. Manag.* 30, 3475–3492. doi: 10.1007/s11269-016-1364-0

Litt, M., Shea, J., Wagnon, P., Steiner, J., Koch, I., Stigter, E., et al. (2019). Glacier ablation and temperature indexed melt models in the Nepalese Himalaya. *Sci. Rep*. 9, 1–13. doi: 10.1038/s41598-019-41657-5

Mahto, S. S., and Mishra, V. (2019). Does ERA-5 outperform other reanalysis products for hydrologic applications in India?. *J. Geophys. Res. Atmos*. 124, 9423–9441. doi: 10.1029/2019JD031155

Mandal, A., Angchuk, T., Azam, M. F., Ramanathan, A., Wagnon, P., Soheb, M. and Singh, C. (2022). 11-year record of wintertime snow surface energy balance and sublimation at 4863 m asl on Chhota Shigri Glacier moraine (western Himalaya, India). *Cryosphere Discuss* 2022, 1–41. doi: 10.5194/tc-2021-386

Mandal, A., Ramanathan, A., Azam, M. F., Angchuk, T., Soheb, M., Kumar, N., et al. (2020). Understanding the interrelationships among mass balance, meteorology, discharge and surface velocity on Chhota Shigri Glacier over 2002–2019 using in situ measurements. *J. Glaciol*. 66, 727–741. doi: 10.1017/jog.2020.42

Maurer, J. M., Schaefer, J. M., Rupper, S., and Corley, A. (2019). Acceleration of ice loss across the Himalayas over the past 40 years. *Sci. Adv*. 5, eaav7266. doi: 10.1126/sciadv.aav7266

Maussion, F., Scherer, D., Mölg, T., Collier, E., Curio, J., and Finkelnburg, R. (2014). Precipitation seasonality and variability over the Tibetan Plateau as resolved by the High Asia Reanalysis. *J. Clim*. 27, 1910–1927. doi: 10.1175/JCLI-D-13-00282.1

Mölg, T., Maussion, F., Yang, W., and Scherer, D. (2012). The footprint of Asian monsoon dynamics in the mass and energy balance of a Tibetan glacier. *Cryosphere* 6, 1445–1461. doi: 10.5194/tc-6-1445-2012

Muhammad, S., and Tian, L. (2016). Changes in the ablation zones of glaciers in the western Himalaya and the Karakoram between 1972 and 2015. *Remote Sens. Environ.* 187, 505–512. doi: 10.1016/j.rse.2016.10.034

Muhammad, S., and Tian, L. (2020). Mass balance and a glacier surge of Guliya ice cap in the western Kunlun Shan between 2005 and 2015. *Remote Sens. Environ*. 244, 111832. doi: 10.1016/j.rse.2020.111832

Muhammad, S., Tian, L., and Khan, A. (2019). Early twenty-first century glacier mass losses in the Indus Basin constrained by density assumptions. *J. Hydrol*. 574, 467–475. doi: 10.1016/j.jhydrol.2019.04.057

Oerlemans, J. (1992). Climate sensitivity of glaciers in southern Norway: application of an energy-balance model to Nigardsbreen, Hellstugubreen and Alfotbreen. *J. Glaciol*. 38, 223–232. doi: 10.1017/S0022143000003634

Oerlemans, J. (2000). Analysis of a 3 year meteorological record from the ablation zone of Morteratschgletscher, Switzerland: energy and mass balance. *J. Glaciol*. 46, 571–579. doi: 10.3189/172756500781832657

Oerlemans, J. (2001). *Glaciers and Climate Change*. Boca Raton: CRC Press.

Oerlemans, J., Anderson, B., Hubbard, A., Huybrechts, P., Johannesson, T., Knap, W. H. (1998). Modeling the response of glaciers to climate warming. *Clim. Dyn*. 14, 267–274. doi: 10.1007/s003820050222

Oerlemans, J., and Knap, W. H. (1998). A 1 year record of global radiation and albedo in the ablation zone of Morteratschgletscher, Switzerland. *J. Glaciol*. 44, 231–238. doi: 10.1017/S0022143000002574

Østrem, G., and Brugman M (1991). *Mass Balance Measurement Techniques*. *A Manual for Field and Office Work*. Saskatoon: Environment Canada.

Patel, A., Goswami, A., Dharpure, J. K., Thamban, M., Sharma, P., Kulkarni, A. V., et al. (2021). Estimation of mass and energy balance of glaciers using a distributed energy balance model over the Chandra river basin (Western Himalaya). *Hydrol. Process.* 35, e14058. doi: 10.1002/hyp.14058

Pellicciotti, F., Helbing, J., Rivera, A., Favier, V., Corripio, J., Araos, J., et al. (2008). A study of the energy balance and melt regime on Juncal Norte Glacier, semi-arid Andes of central Chile, using melt models of different complexity. *Hydrol. Process.* 22, 3980–3997. doi: 10.1002/hyp.7085

Pratap, B., Dobhal, D. P., Mehta, M., and Bhambri, R. (2015). Influence of debris cover and altitude on glacier surface melting: a case study on Dokriani Glacier, central Himalaya, India. *Ann. Glaciol*. 56, 9–16. doi: 10.3189/2015AoG70A971

Ragettli, S., Pellicciotti, F., Bordoy, R., and Immerzeel, W. W. (2013). Sources of uncertainty in modeling the glaciohydrological response of a Karakoram watershed to climate change. *Water Resour. Res*. 49, 6048–6066. doi: 10.1002/wrcr.20450

Ragettli, S., Pellicciotti, F., Immerzeel, W. W., Miles, E. S., Petersen, L., Heynen, M., et al. (2015). Unraveling the hydrology of a Himalayan catchment through integration of high resolution in situ data and Remote Sens. with an advanced simulation model. *Adv. Water Resour*. 78, 94–111. doi: 10.1016/j.advwatres.2015.01.013

Ramsankaran, R. A. A. J., Pandit, A., and Azam, M. F. (2018). Spatially distributed ice-thickness modelling for Chhota Shigri Glacier in western Himalayas, India. *Int. J. Remote Sens*. 39, 3320–3343. doi: 10.1080/01431161.2018.1441563

Rashid, I., and Majeed, U. (2020). Retreat and geodetic mass changes of Zemu Glacier, Sikkim Himalaya, India, between 1931 and 2018. *Reg. Environ. Change* 20, 1–13. doi: 10.1007/s10113-020-01717-3

Rounce, D. R., Khurana, T., Short, M. B., Hock, R., Shean, D. E., and Brinkerhoff, D. J. (2020). Quantifying parameter uncertainty in a large-scale glacier

evolution model using Bayesian inference: application to High Mountain Asia. *J. Glaciol*. 66, 175–187. doi: 10.1017/jog.2019.91

Sakai, A., Nuimura, T., Fujita, K., Takenaka, S., Nagai, H., and Lamsal, D. (2015). Climate regime of Asian glaciers revealed by GAMDAM glacier inventory. *Cryosphere* 9, 865–880. doi: 10.5194/tc-9-865-2015

Shea, J. M., Immerzeel, W. W., Wagnon, P., Vincent, C., and Bajracharya, S. (2015a). Modelling glacier change in the Everest region, Nepal Himalaya. *Cryosphere* 9, 1105–1128. doi: 10.5194/tc-9-1105-2015

Shea, J. M., Wagnon, P., Immerzeel, W. W., Biron, R., Brun, F., and Pellicciotti, F. (2015b). A comparative high-altitude meteorological analysis from three catchments in the Nepalese Himalaya. *Int. J. Water Resour. Dev*. 31, 174–200. doi: 10.1080/07900627.2015.1020417

Shean, D. E., Bhushan, S., Montesano, P., Rounce, D. R., Arendt, A., and Osmanoglu, B. (2020). A systematic, regional assessment of high mountain Asia glacier mass balance. *Front. Earth Sci*. 7, 363. doi: 10.3389/feart.2019.00363

Sicart, J. E., Wagnon, P., and Ribstein, P. (2005). Atmospheric controls of the heat balance of Zongo Glacier (16 S, Bolivia). *J. Geophys. Res. Atmos*. 110, D12. doi: 10.1029/2004JD005732

Singh, N., Singhal, M., Chhikara, S., Karakoti, I., Chauhan, P. and Dobhal, D. P. (2020). Radiation and energy balance dynamics over a rapidly receding glacier in the central Himalaya. *Int. J. Climatol.* 40, 400–420. doi: 10.1002/joc.6218

Soheb, M., Ramanathan, A. L., Pandey, M., and Vatsal, S. (2017). "Change in volume of glaciers and glacierets in two catchments of Western Himalayas, India Since 1993–2015," in *Geospatial Applications for Natural Resources Management*. Boca Raton: CRC Press Taylor and Francis, 123–130.

Srivastava, S., Garg, P. K., and Azam, M. (2021). Seven decades of dimensional and mass balance changes on Dokriani Bamak and Chhota Shigri Glaciers, Indian Himalaya, using satellite data and modelling. *J. Indian Soc. Remote. Sens.* 50, 1–18. doi: 10.1007/s12524-021-01455-x

Stigter, E. E., Litt, M., Steiner, J. F., Bonekamp, P. N., Shea, J. M., Bierkens, M. F., et al. (2018). The importance of snow sublimation on a Himalayan glacier. *Front. Earth Sci*. 6, 108. doi: 10.3389/feart.2018.00108

Stigter, E. E., Steiner, J. F., Koch, I., Saloranta, T. M., Kirkham, J. D., and Immerzeel, W. W. (2021). Energy and mass balance dynamics of the seasonal snowpack at two high-altitude sites in the Himalaya. *Cold Reg Sci Technol*. 183, 103233. doi: 10.1016/j.coldregions.2021.103233

Sun, W., Qin, X., Du, W., Liu, W., Liu, Y., Zhang, T., et al. (2014). Ablation modeling and surface energy budget in the ablation zone of Laohugou glacier No. 12, western Qilian mountains, China. *Ann. Glaciol.* 55, 111–120. doi: 10.3189/2014AoG66A902

Sunako, S., Fujita, K., Sakai, A., and Kayastha, R. B. (2019). Mass balance of Trambau Glacier, Rolwaling region, Nepal Himalaya: *in-situ* observations, long-term reconstruction and mass-balance sensitivity. *J. Glaciol*. 65, 605–616. doi: 10.1017/jog.2019.37

Tawde, S. A., Kulkarni, A. V., and Bala, G. (2017). An estimate of glacier mass balance for the Chandra basin, western Himalaya, for the period 1984–2012. *Ann. Glaciol*. 58, 99–109. doi: 10.1017/aog.2017.18

Vashisht, P., Pandey, M., Ramanathan, A. L., Tayal, S., and Jackson, M. (2017). Comparative assessment of volume change in Kolahoi and Chhota Shigri Glaciers, Western Himalayas, using empirical techniques. *J. Clim. Change* 3, 37–48. doi: 10.3233/JCC-170004

Verma, A., Kumar, A., Gupta, A. K., Tiwari, S. K., Bhambri, R., and Naithani, S. (2018). Hydroclimatic significance of stable isotopes in precipitation from glaciers of Garhwal Himalaya, Upper Ganga Basin (UGB), India. *Hydrol. Process*. 32, 1874–1893. doi: 10.1002/hyp.13128

Vijay, S., and Braun, M. (2016). Elevation change rates of glaciers in the Lahaul-Spiti (Western Himalaya, India) during 2000–2012 and 2012–2013. *Remote Sens*. 8, 1038. doi: 10.3390/rs8121038

Vijay, S., and Braun, M. (2018). Early 21st century spatially detailed elevation changes of Jammu and Kashmir glaciers (Karakoram–Himalaya). *Glob. Planet. Change* 165, 137–146. doi: 10.1016/j.gloplacha.2018.03.014

Vincent, C., Kappenberger, G., Valla, F., Bauder, A., Funk, M., and Le Meur, E. (2004). Ice ablation as evidence of climate change in the Alps over the 20th century. *J. Geophys. Res. Atmos*. 109, D10. doi: 10.1029/2003JD003857

Vincent, C., Ramanathan, A., Wagnon, P., Dobhal, D. P., Linda, A., Berthier, E., et al. (2013). Balanced conditions or slight mass gain of glaciers in the Lahaul and Spiti region (northern India, Himalaya) during the nineties preceded recent mass loss. *Cryosphere* 7, 569–582. doi: 10.5194/tc-7-569-2013

Vincent, C., Wagnon, P., Shea, J. M., Immerzeel, W. W., Kraaijenbrink, P., Shrestha, D., et al. (2016). Reduced melt on debris-covered glaciers: investigations from Changri Nup Glacier, Nepal. *Cryosphere* 10, 1845–1858. doi: 10.5194/tc-10-1845-2016

Wagnon, P., Linda, A., Arnaud, Y., Kumar, R., Sharma, P., Vincent, C., et al. (2007). Four years of mass balance on Chhota Shigri Glacier, Himachal Pradesh, India, a new benchmark glacier in the western Himalaya. *J. Glaciol*. 53, 603–611. doi: 10.3189/002214307784409306

Wagnon, P., Ribstein, P., Kaser, G., and Berton, P. (1999). Energy balance and runoff seasonality of a Bolivian glacier. *Glob. Planet. Change* 22, 49–58. doi: 10.1016/S0921-8181(99)00025-9

Wagnon, P., Sicart, J. E., Berthier, E., and Chazarin, J. P. (2003). Wintertime high-altitude surface energy balance of a Bolivian glacier, Illimani, 6340 m above sea level. *J. Geophys. Res. Atmos*. 108(D6). doi: 10.1029/2002JD002088

Yadav, J. S., Misra, A., Dobhal, D. P., Yadav, R. B. S., and Upadhyay, R. (2021). Snow cover mapping, topographic controls and integration of meteorological data sets in Din-Gad Basin, Central Himalaya. *Quat. Int*. 575, 160–177. doi: 10.1016/j.quaint.2020.05.030

Yadav, J. S., Pratap, B., Gupta, A. K., Dobhal, D. P., Yadav, R. B. S., and Tiwari, S. K. (2019). Spatio-temporal variability of near-surface air temperature in the Dokriani glacier catchment (DGC), central Himalaya. *Theor. Appl. Climatol*. 136, 1513–1532. doi: 10.1007/s00704-018-2544-z

Zhang, Y., Fujita, K., Liu, S., Liu, Q., and Nuimura, T. (2011). Distribution of debris thickness and its effect on ice melt at Hailuogou glacier, southeastern Tibetan Plateau, using in situ surveys and ASTER imagery. J. *Glaciol*. 57, 1147–1157. doi: 10.3189/002214311798843331

Conflict of Interest: The authors declare that the research was conducted in the absence of any commercial or financial relationships that could be construed as a potential conflict of interest.